PYTA: A Universal Chelator for Advancing the Theranostic Palette of Nuclear Medicine

Megan E. Simms,[a†‡] Zhiyao Li,[b,c‡] Megan M. Sibley,[a] Alexander S. Ivanov,[a] Caroline M. Lara,[d] Timothy C. Johnstone,[e] Vilmos Kertesz,[f] Amanda Fears,[b,c] Frankie D. White,[g*] Daniel L. J. Thorek,[b,c,h,i*] Nikki A. Thiele[a*]

[a]Chemical Sciences Division, Oak Ridge National Laboratory, Oak Ridge, TN 37831, United States. E-mail: thielena@ornl.gov
[b]Department of Radiology, Washington University in St. Louis School of Medicine, St. Louis, MO 63110, United States. E-mail: thorekd@wustl.edu
[c]Program in Quantitative Molecular Therapeutics, Washington University in St. Louis School of Medicine, St. Louis, MO 63110, United States
[d]Department of Biological Sciences, University of Notre Dame, Notre Dame, IN 46556, United States
[e]Department of Chemistry and Biochemistry, University of California Santa Cruz, Santa Cruz, CA 95064, United States
[f]Biosciences Division, Oak Ridge National Laboratory, Oak Ridge, TN 37831, United States
[g]Radioisotope Science and Technology Division, Oak Ridge National Laboratory, Oak Ridge, TN 37831, United States. E-mail: whitefd@ornl.gov
[h]Department of Biomedical Engineering, Washington University in St. Louis, St. Louis, MO 63110, United States
[i]Oncologic Imaging Program, Siteman Cancer Center, Washington University in St. Louis School of Medicine, St. Louis, MO 63110, United States

[‡]These authors contributed equally
*E-mail: thielena@ornl.gov, thorekd@wustl.edu, whitefd@ornl.gov

TABLE OF CONTENTS

LIST OF TABLES

LIST OF FIGURES

Figure page

1. General Materials and Methods

Caution! The isotopes ^{225}Ac, ^{177}Lu, ^{111}In, and ^{44}Sc are radioactive. Work should only be performed by trained personnel in facilities equipped to safely handle and store these materials.

All solvents and reagents were of ACS grade or higher and were purchased from commercial sources. Deionized water (≥18 MΩ·cm) was obtained from a Milli-Q Reference water purification system. 1,4,7,10-Tetraazacyclododecane-*N*,*N*′,*N*″,*N*‴-tetraacetic acid (DOTA, min. 98%) was purchased from Strem (Newburyport, MA, USA) and used as received. Macropa·2HCl·1.5H_2O was prepared according to published literature procedures[1–3] and recrystallized four times from 6 M HCl (Optima HCl and ultra-trace elemental analysis grade H_2O, Fisher Scientific, Pittsburgh, PA, USA) by precipitation with acetone. PYTA was prepared as described previously[4] starting from py_2[18]aneN_6·0.2HCl·3.8HBr·0.5H_2O,[5] with slight modifications. Specifically, 4.3 equiv of ethyl bromoacetate and 12 equiv of Na_2CO_3 were used in the alkylation reaction. Following extraction, the crude material was heated for 2 days (unoptimized) in 6 M HCl at 90 °C to hydrolyze the ester groups. Purification of the product was achieved by semi-preparative reverse-phase C_{18} high-performance liquid chromatography (HPLC, Shimadzu, Kyoto, Japan) using a Restek Ultra Aqueous column (100 Å, 5 μm, 250 mm × 21.2 mm, Bellefonte, PA) and a MeOH/H_2O mobile phase containing 0.1% trifluoroacetic acid. PYTA·3.8 CF_3COOH was isolated as a white powder (1.347 g, 61% yield). The number of TFA counteranions per ligand varied slightly from batch to batch and is noted for each experiment. The purity and composition of macropa and PYTA were verified to be >99% by reverse-phase C_{18} analytical HPLC (Shimadzu HPLC; Restek Ultra Aqueous C18 column, 100 Å, 5 μm, 250 mm × 4.6 mm), elemental analysis (Atlantic Microlab, Norcross, GA, USA), and ^1H and $^{13}C\{^1H\}$ nuclear magnetic resonance (NMR) spectroscopy (Avance III 400 MHz spectrometer equipped with a BBO probe, Bruker, Billerica, MA, USA). Spectra are provided in Appendix A of the Supporting Information. Chemical shifts are reported in parts per million (ppm). Spectra acquired in CD_3OD were referenced to a tetramethylsilane internal standard (0 ppm). Samples prepared in D_2O were spiked with CH_3CN, and the spectra were referenced to the corresponding signal at either 2.06 ppm (^1H) or 1.47 ppm (^{13}C). High-resolution mass spectra (HRMS) were obtained on a Q Exactive HF Orbitrap mass spectrometer (Thermo Scientific, Waltham, MA, USA) at 240,000 resolution in positive electrospray ionization (ESI) mode. Samples were introduced using an Open Port Sampling Interface (OPSI) on the instrument.

2. Computational Chemistry

Vienna *ab initio* simulation package (VASP)[6,7] was used to perform crystal structure calculations and ab initio molecular dynamics (AIMD) simulations using density functional theory (DFT). The valence electronic states were expanded on a basis of plane waves, while the core valence interactions were described using the Projector Augmented Wave (PAW) approach and standard PAW potentials were used.[8,9] The plane wave kinetic energy cutoff was set to 650 eV and the PBE GGA functional[10] was employed to describe the exchange-correlation interactions. The Brillouin zone was sampled using a well converged Gamma centered (2×1×1) *k*-point mesh for the crystal structure calculations, while the Gamma point approximation was used for the AIMD simulations. The DFT-D3 approach of Grimme[11] was used to account for the van der Waals interactions.

Cell and structural optimizations of [La(H_2PYTA)](NO_3)·3H_2O and [Ac(H_2PYTA)](NO_3)·3H_2O were carried out starting from the corresponding single-crystal XRD structure of the La complex.[4]

Since the position of hydrogen atoms were not resolved in the experimental crystal structure, they were placed in idealized positions using the Mercury program[12] developed by the Cambridge Crystallographic Data Centre (CCDC). The SCF convergence threshold was set to 10^{-5} eV and a Pulay scheme[13] was used for charge density mixing during the SCF solution. A comparison between the DFT-optimized structural parameters and experimental data is provided in Table S1. The DFT-optimized bond lengths between La^{3+} and PYTA donor atoms showed good agreement with the experimental XRD data, validating the chosen level of theory. This level of theory was used to calculate a hypothetical crystal structure of the isostructural complex with Ac^{3+}. The DFT-predicted Ac–O and Ac–N bonds in the complex were found to be only slightly longer than the La–O and La–N bonds, consistent with the slightly larger ionic radius of Ac^{3+}. These results suggest that in the solid state, Ac^{3+}–PYTA structural characteristics can be approximated to some degree by the La^{3+}–PYTA surrogate crystal structure.

For the AIMD simulations, the initial structure of the $[La(PYTA)]^-$/$[Ac(PYTA)]^-$ complex–water system (a periodic cubic box of 15 Å length containing one complex and 75 water molecules) was pre-equilibrated for 3 nanoseconds in a canonical ensemble at a temperature of 300 K using the extended PCFF force field[14] supported in MedeA-LAMMPS (MedeA®-2.20, Materials Design, Inc., Angel Fire, NM, USA, 2016).[15,16] AIMD simulations at 300 K were performed using the Nosé–Hoover thermostat[16] with a time step of 1 femtosecond. After equilibrating for 5 picoseconds (ps), the AIMD trajectory was collected for 20 ps and used for the radial distribution function analysis. The results are summarized in Figure S2. As expected based on the larger ionic radius of Ac^{3+} versus La^{3+}, the AIMD simulations predicted a slightly longer average Ac–O bond length of 2.65 Å in comparison to the average La–O distance (2.55 Å). Notably, all four carboxylate groups remain coordinated to the metal center over the course of 20 ps, supporting the notion that the La^{3+} complex approximates the Ac^{3+} complex in solution.

3. Solution-State Chemistry

A stock solution of PYTA (4 mM) was prepared by massing PYTA·3.8 CF_3COOH (19.8 mg, 0.02 mmol) into a 5 mL volumetric flask. The solid was dissolved in D_2O (1 mL) and lyophilized. This step was repeated once more. Then, the sample was diluted to 5 mL with D_2O. Using the same procedure, a stock solution of NaOD (1 M) was prepared in D_2O from semiconductor grade NaOH (Sigma Aldrich, 99.99%). Metal stock solutions (10 mM) were prepared in D_2O from their chloride salts ($LaCl_3·7H_2O$, Alfa Aesar 99.99%; $LuCl_3·6H_2O$, Thermo Scientific 99.9%; anhydrous $ScCl_3$, Aldrich 99.9%; $InCl_3·xH_2O$, Alfa Aesar 99.99%). The exact concentrations of these solutions were determined in quadruplicate by complexometric titration with a standardized solution of Na_2EDTA, using xylenol orange as an indicator.

NMR samples of La–, Lu–, In–, and Sc–PYTA (2 mM) were prepared by combining PYTA (300 µL, 1.2 µmol), metal ion (113.8–151.8 µL, 1.26 µmol), and CH_3CN (0.6 µmol as an internal standard) in a vial. The total volume was brought to 0.600 mL with D_2O. Then, the pD of each solution was carefully adjusted to ~7 using 1 M NaOD. The samples were allowed to stand for 1 h at ambient temperature (~18 °C), and then the ^1H NMR spectra were collected. The H_2O signal was suppressed in these spectra using a presaturation pulse sequence. The La^{3+} sample was further heated at 60 °C for 20 h, and the ^1H NMR spectrum was re-acquired. Variable temperature ^1H NMR spectra for the In^{3+} sample were obtained at 25, 40, 60, 70, 80, 90 °C, with a 10 min equilibration time between each temperature change and spectral acquisition. The sample was then returned to 25 °C and the ^1H spectrum was re-acquired to ensure that it matched the spectrum of the sample prior to heating.

4. Solid-State Chemistry

4.1 Synthesis of In–PYTA complex

PYTA·2.5 CF_3COOH (21.0 mg; 0.025 mmol), triethylamine (10.7 µL; 0.077 mmol), and EtOH (5 mL) were combined in a vial. The resulting solution was heated to 60 °C. Then, a solution of $In(ClO_4)_3·8H_2O$ (13.8 mg; 0.025 mmol) in EtOH (3 mL) was added dropwise. A white precipitate formed immediately. The suspension was stirred at 60 °C for 1 h and then concentrated to ~1 mL. An aliquot of H_2O (3 mL) was added to the suspension, and it was heated at 70 °C until dissolution of the precipitate was complete (~1 h). Crystals suitable for single-crystal X-ray diffraction were obtained from slow evaporation of this solution after several days and were determined to have the composition $[In(H_2PYTA)]ClO_4$.

4.2 Synthesis of Sc–PYTA complex

PYTA·3.8 CF_3COOH (22.4 mg; 0.023 mmol), triethylamine (10.7 µL; 0.077 mmol), and EtOH (3 mL) were combined in a vial. To this solution was added $Sc(ClO_4)_3·6H_2O$ (50 wt% in H_2O; 19.7 mg; 0.022 mmol) in EtOH (3 mL). White precipitate formed immediately. The precipitate was isolated via centrifugation, washed with EtOH (6 mL), and then dissolved in H_2O (5 mL) with gentle heating (~40 °C). The aqueous solution was then concentrated at 60 °C to ~2 mL. Crystals suitable for single-crystal X-ray diffraction were obtained from slow evaporation of this solution after 1 week and were determined to have the composition $[Sc(HPYTA)]·3H_2O$.

4.3 Synthesis of Cu–PYTA complex

PYTA·3.8 CF_3COOH (20.1 mg; 0.021 mmol), triethylamine (10.7 µL; 0.077 mmol) and EtOH (3 mL) were combined in a vial. The solution was heated at 70 °C for 15 min. To this solution was added $Cu(ClO_4)_2·6H_2O$ (11.8 mg; 0.032 mmol) in EtOH (3 mL). The reaction solution immediately turned green. The reaction volume was reduced to ~3 mL. Crystals suitable for single-crystal X-ray diffraction were obtained from slow evaporation after ~2 weeks and were determined to have the composition $[Cu(H_2PYTA)]·2H_2O$.

4.4 X-ray diffraction and refinement

X-ray diffraction measurements were performed on a Bruker D8 Venture diffractometer equipped with an IµS 3.0 molybdenum X-ray source (λ = 0.71073 Å). An Oxford Cryostream 800 was used to perform the data collection at room temperature. Apex IV software was used for data collection and unit cell determination. The crystal structures were solved using SHELXT and refined using SHELXL within the *OLEX2* GUI.[17,18] Non-hydrogen atoms were refined anisotropically. Hydrogen atoms bound to carbon were included in the model at geometrically calculated positions and refined using a riding model. Hydrogen atoms bound to heteroatoms were located in the Fourier electron density difference map and, unless otherwise noted, refined semi-freely with the use of temperature-appropriate distance restraints and coupled displacement parameters. The CIF files within this report were archived in the Cambridge Crystallographic Data Centre under CCDC deposition numbers 2297429, 2297430, and 2339314. Crystallographic data collection and refinement parameters are collected in Table S2 of Section S8 of the Supporting Information.

For the In–PYTA structure, the In complex resides on a crystallographic two-fold rotation axis, allowing the complex to assume its full C_2 molecular point-group symmetry in the solid state. The perchlorate anion was disordered about a two-fold axis with the chlorine atoms lying close to, but

not on, this special position. Because of the resulting proximity of the disordered oxygen atoms, distance restraints were employed. The Cl–O bond lengths and O···O distances were collectively refined using a single free variable given the geometric relationship for tetrahedra whereby the edge length is 1.633 times the length of the circumradius, i.e., Cl–O = 1.633(O···O). Rigid-bond and similarity restraints were also applied to the anisotropic displacement parameters of the atoms in the disordered anion. The disordered contents of channels that run through the crystal parallel to *c* and along the *R*-centered $\bar{3}$ rotoinversion axes were masked.

For the Sc–PYTA structure, the pendent carboxylic acid was disordered across two positions. The hydrogen-bearing oxygen atoms were confirmed to be those with the longer C–O bond lengths Refinement of these hydrogen atoms was performed using an idealized tetrahedral C–O–H angle and a constrained O–H distance of 0.82 Å, but free rotation was allowed about the C–O bond axis. The final position of this hydrogen atom afforded a coherent hydrogen-bonding network in the crystal. The final positions of the hydrogen atoms of the water molecules were also confirmed to form a coherent hydrogen-bonding pattern.

For the Cu–PYTA structure, a lower symmetry, monoclinic space group *C*2/*c*, like that observed for Sc–PYTA, was obtained. Two of the four carboxylic acids of PYTA are deprotonated, giving rise to an overall neutral Cu^{2+} complex. The outer-sphere crystal structure environment of Cu–PYTA consists of four water molecules in which the hydrogen atoms were freely refined. These water molecules form a coherent hydrogen-bonding pattern with the hydrogens of the carboxylic acid groups.

5. Radionuclides

5.1 Sourcing and solution preparation

Actinium-225 (^{225}Ac) was obtained from a ^{229}Th generator at Oak Ridge National Laboratory and received as a dried-down nitrate salt with a specific activity of 5.80×10^4 Ci/g (carrier free) and a radionuclidic purity of 99.99%. Upon receipt, it was reconstituted in 10 mM HCl (Fisher Optima HCl and Fisher ultra-trace elemental analysis grade H_2O) to yield a stock solution of approximately 74 kBq ^{225}Ac/μL (2 μCi ^{225}Ac/μL). From this stock solution, working solutions of 0.93–1.11 kBq/μL (0.025–0.03 μCi/μL) or 3.7 kBq/μL (0.1 μCi/μL) were prepared prior to radiolabeling and serum stability experiments, respectively, by further dilution with 10 mM HCl.

Lutetium-177 (^{177}Lu) was produced at the Missouri University Research Reactor (MURR) and purchased from the National Isotope Development Center (NIDC). It was received as a chloride solution (0.05 M HCl) with a specific activity ≥740 GBq/mg (≥20 Ci/mg) and a radionuclidic purity of ≥99%. From this stock solution, working solutions of 2.2–3.7 kBq/μL (0.06–0.1 μCi/μL) or 14.8 kBq/μL (0.4 μCi/μL) were prepared prior to radiolabeling and serum stability experiments, respectively, by further dilution with 10 mM HCl.

Indium-111 (^{111}In) was purchased from BWXT Medical (Vancouver, BC) and received as a chloride solution (0.05 M HCl) with a specific activity >50 Ci/mg, an activity concentration of approximately 1,000 mCi/mL, and a radionuclidic purity of >99.9%. From this stock solution, working solutions of 7.4–11.1 kBq/μL (0.2–0.3 μCi/μL) or 18.5–29.6 kBq/μL (0.5–0.8 μCi/μL) were prepared prior to radiolabeling and serum stability experiments, respectively, by further dilution with 10 mM HCl.

Scandium-44 (^{44}Sc) was eluted in 0.05 M HCl from a ^{44}Ti/^{44}Sc generator as described in detail previously,[19] provided by the Department of Energy, yielding a stock solution of 1.8 (±0.09) mCi in 3.6 mL (0.5 μCi/μL, 18.5 kBq/μL). The pH of the stock solution was adjusted to approximately 4.5 through addition of 5 M NaOH (25 μL) and NH_4OAc (0.25 M, pH 4.05). This solution was used for the labeling experiments below.

5.2 Gamma spectroscopy

The radionuclidic purity and activity of ^{225}Ac, ^{177}Lu, and ^{111}In solutions were verified by gamma spectroscopy using a Gamma Analyst Integrated Gamma Spectrometer (Canberra), which consists of a high-purity germanium (HPGe) detector (model GC-GA1), U-type cryostat, and automatic sample changer. The detector energy and efficiency were calibrated using a mixed gamma point source containing ^{57}Co, ^{60}Co, ^{88}Y, ^{109}Cd, ^{113}Sn, ^{137}Cs, ^{139}Ce, ^{203}Hg, and ^{241}Am, traceable to the National Institute of Standards and Technology (NIST) and supplied by Eckert & Ziegler Analytics (Atlanta, GA, USA). Samples to be counted were prepared by adding 10 μL of working solution into 12 × 75 mm polypropylene test tubes. Counting dead time was maintained below 5% for all measurements. Data was analyzed using Genie 2000 software (v3.2.1 Canberra). Spectral acquisitions of ^{44}Sc were made for 1 h on a HPGe system (GEM-50195-S and Gamma-Vision v8.0, Ametek). Samples were placed 5 cm offset from the aluminum endcap, enclosed in a 10 cm lead shield (HPLBS1, Ametek). The spectra of these samples can be found in Appendix B of the Supporting Information (Figures B1–B4).

6. Radiolabeling and Serum Stability Studies

6.1 General

Stock solutions of PYTA, macropa, and DOTA were prepared in Milli-Q H_2O. The concentration of each solution was verified by potentiometric titration. Subsequently, the stocks were serially diluted with H_2O to afford a series of ligand solutions ranging from 1.5×10^{-7} to 1.5×10^{-2} M. NH_4OAc buffer (0.5 M, pH 6.0) was prepared using solid NH_4OAc (99.999% trace metals basis, Sigma-Aldrich) and glacial HOAc (≥99%, Sigma-Aldrich), and was rendered metal-free by contact with Chelex (5 g/L) overnight via the batch method. It was subsequently filtered through a polypropylene column equipped with a 20 μm polyethylene frit and stored in an acid-washed plastic bottle. Human serum from male AB plasma (USA origin, sterile-filtered) was purchased from Sigma-Aldrich. The following plate/mobile phase systems were used for radio thin-layer chromatography (radio-TLC):

TLC System A: Mobile phase: 50 mM ethylenediaminetetraacetic acid (EDTA) at pH 6.0, prepared by dissolving a suspension of H_4EDTA (99.995% trace metals basis, Sigma-Aldrich) in Milli-Q H_2O with NaOH. TLC plate: instant thin layer chromatography-silica gel (iTLC-SG) plates (Agilent).

TLC System B: Mobile phase: 0.4 M sodium citrate with 10% MeOH, prepared by mixing sodium citrate buffer (0.4 M, pH 6) with MeOH (9:1 v/v). TLC plate: aluminum-backed silica TLC plates (alumTLC-SG, silica gel 60, F254, Merck).

TLC System C: Mobile phase: 10 mM ammonium acetate:MeOH (9:1 v/v). TLC plate: aluminum-backed reverse-phase TLC plates (alumTLC-RP, silica gel 60, RP-18, F254, Merck).

TLC System D: Mobile phase: 50 mM EDTA at pH 5.5. TLC plate: instant thin layer chromatography-silica gel (iTLC-SG) plates (Gelman Sciences).

TLC System E: Mobile phase: saline. TLC plate: instant thin layer chromatography-silica gel (iTLC-SG) plates (Gelman Sciences).

TLC System F: Mobile phase: 0.4 M sodium citrate with 10% MeOH, prepared by mixing sodium citrate buffer (0.4 M, pH 6) with MeOH (9:1 v/v). TLC plate: aluminum-backed reverse-phase TLC plates (alumTLC-RP, silica gel 60, RP-18, F254, Merck).

6.2 Concentration-dependent radiolabeling

Radiolabeling experiments with ^{225}Ac, ^{177}Lu, ^{111}In, and ^{44}Sc were performed in triplicate at each chelator concentration by addition of chelator (10 μL) and radionuclide working solution (10 μL; 9.3–11.1 kBq ^{225}Ac, 22–37 kBq ^{177}Lu, 74–111 kBq ^{111}In, or 185 kBq ^{44}Sc) to polypropylene screw-capped tubes containing pH 6 NH_4OAc buffer (130 μL), giving a final chelator concentration of 10^{-8} –10^{-3} M. Control samples were also prepared in which chelator was substituted with H_2O. The samples were shaken to ensure complete mixing and then incubated at room temperature for 5 min. After removing an aliquot for radio-TLC, the samples were rotated end-over-end in an incubator at 25 °C until the next time point (60 min). Radiolabeling of DOTA at 80 °C was also performed for comparison. The pH of representative samples was confirmed to be 6 by spotting an aliquot (1 μL) onto a pH indicator strip. Additionally, radiolabeling experiments with 1.665 MBq of ^{44}Sc were executed for PYTA in triplicate in an analogous manner, except the final reaction volume was 100 μL, the final pH was approximately 4.5, and the mixing time was 30 min.

The radiolabeling progress was analyzed via radio-TLC by spotting an aliquot (5 μL) of reaction solution onto iTLC-SG, alumTLC-SG, or alumTLC-RP plates and developing them using the mobile phases described above. Retention factors (R_f) are provided in Table S3. Representative examples of developed TLC plates are shown in Figures S10–S23. For ^{225}Ac radio-TLC, strips were analyzed approximately 24 h after their development to allow sufficient time for radioactive equilibrium to be reached between ^{225}Ac and its decay chain. ^{177}Lu, ^{111}In, and ^{44}Sc radio-TLC strips were analyzed immediately. TLC imaging was performed using an AR-2000 scanner system equipped with P-10 gas and either *WinScan 3* or *WinScan 2D* imaging software (Eckert & Ziegler Radiopharma Inc). Radiochemical yields (RCYs) were calculated by dividing the counts associated with complexed radionuclide by the total counts integrated along the length of the TLC plate.

6.3 Serum challenges

Chelators were radiolabeled at the concentrations indicated in Table S4 for 60 min at 25 °C (PYTA, macropa) or 80 °C (DOTA) with ^{225}Ac (37 kBq), ^{177}Lu (148 kBq), ^{111}In (185–296 kBq), or ^{44}Sc (740 kBq, PYTA only) in pH 6.0 HOAc-NH_4OAc buffer (150 μL final volume). Each concentration of chelator was selected based on the lowest concentration that gave quantitative or nearly quantitative RCYs in radiolabeling experiments (Section 6.2), multiplied by a factor of 4 to account for subsequent dilution by serum. RCYs of >97% were confirmed by radio-TLC for all radiolabeling reactions except for the [^{177}Lu]Lu–macropa reaction, which had a RCY of 82%. Next, an aliquot of human serum (450 μL) was added to each sample, yielding a final reaction volume of 600 μL and final chelator concentrations ranging from 1×10^{-5} M to 1×10^{-3} M (Table S4). Control samples were also prepared in which chelator was substituted with H_2O and diluted with 450 μL of serum. The samples were rotated end-over-end at 37 °C and sampled at predetermined time points. The percentage of intact complex was determined by radio-TLC, as described in Section 6.2 above. The final pH of representative samples was determined to be 7 by spotting an aliquot (1 μL) of reaction solution onto a pH indicator strip.

7. PET Imaging and Ex Vivo Biodistribution

7.1 General

All radioactive material handling and animal experimentation were conducted in compliance with institutional regulations and approved by Environmental Health and Safety Radioactive Materials protocol #1169-01 and Institutional Animal Care and Use Committee protocol #22-0023. Female Swiss Webster mice (6–8 weeks, from Charles River Laboratories) were purchased for imaging and biodistribution studies. A total of 16 mice were used for the biodistribution study of the ^{225}Ac–PYTA complex and 12 mice for the [^{44}Sc]Sc–PYTA complex, with n = 4 per time point. Additionally, 4 mice were used for the [^{44}Sc]Sc–PYTA PET imaging study.

7.2 ^{225}Ac studies

PYTA (1×10^{-3} M) was radiolabeled with ^{225}Ac (185 kBq, 5 μCi) at room temperature in NH_4OAc buffer (0.25 M, pH 6) containing gentisic acid (1 mM) and ascorbic acid (1 mM). The final volume of the reaction solution was 500 μL. After 60 min, the reaction was spotted onto an alumTLC-SG strip and developed using TLC system B, which confirmed >98% RCY. The reaction was allowed to proceed for 48 h and then re-sampled, and the RCY was again confirmed to be >98%. At this time, the reaction solution was diluted 10-fold with saline for intravenous administration. Mice were anesthetized by isoflurane in air (2%, 2 L/min), and approximately 100 μL (~3.7 kBq, 100 nCi) of ^{225}Ac complex was administered intravenously to mice by retro-orbital injection. Each group was sacrificed after 15 min, 1 h, 24 h, or 48 h post-injection. Selected tissues and biological fluids were collected, weighed, and gamma counted at equilibrium (>4 h). Counts were decay corrected from the time of injection and then converted to the percentage of injected activity (% IA) per gram of weighed tissue (% IA/g).

7.3 ^{44}Sc studies

PYTA (5.7 mM, 15 μL) was radiolabeled with ^{44}Sc (33.5 MBq, 906 μCi) at room temperature in NH_4OAc buffer (0.25 M, pH 6). The final volume of the reaction solution was 1.5 mL. After 40 min, the reaction was spotted onto an alumTLC-RP strip and developed using TLC system C, which confirmed >98% RCY. After the reaction, a Sep-Pak C18 cartridge (Waters) was used to purify the final compound. The labeled compound was eluted using EtOH and diluted with saline for intravenous administration. Radiolabeled solutions were prepared fresh for PET imaging and biodistribution studies, which were carried out on different days. Mice were anesthetized by isoflurane in air (2%, 2 L/min), and approximately 100 μL (~5.18 MBq, 140 μCi) of ^{44}Sc complex was administered to mice by intravenous tail vein catheter for dynamic imaging. Animals were imaged using the microPET R4 (Siemens) and data was corrected for detector non-uniformity, dead time, random coincidences and physical decay. An energy window of 350–650 keV and coincidence-timing window of 6 ns was used. Activity concentration calibrated data was reconstructed and visualized using ASIProVM (Siemens). Animals for biodistribution were administered activity intravenously by the retroorbital sinus (~2.775 MBq, 75 μCi in 100 μL) and were sacrificed after 15 min, 1 h, or 4 h post-injection (n = 4 per time point). Selected tissues and biological fluids were collected, weighed, and gamma counted. Counts were decay corrected from the time of injection and then converted to the percentage of injected activity (% IA) per gram of weighed tissue (% IA/g) determined by automated microbalance.

8. Supporting Figures, Tables, and Schemes

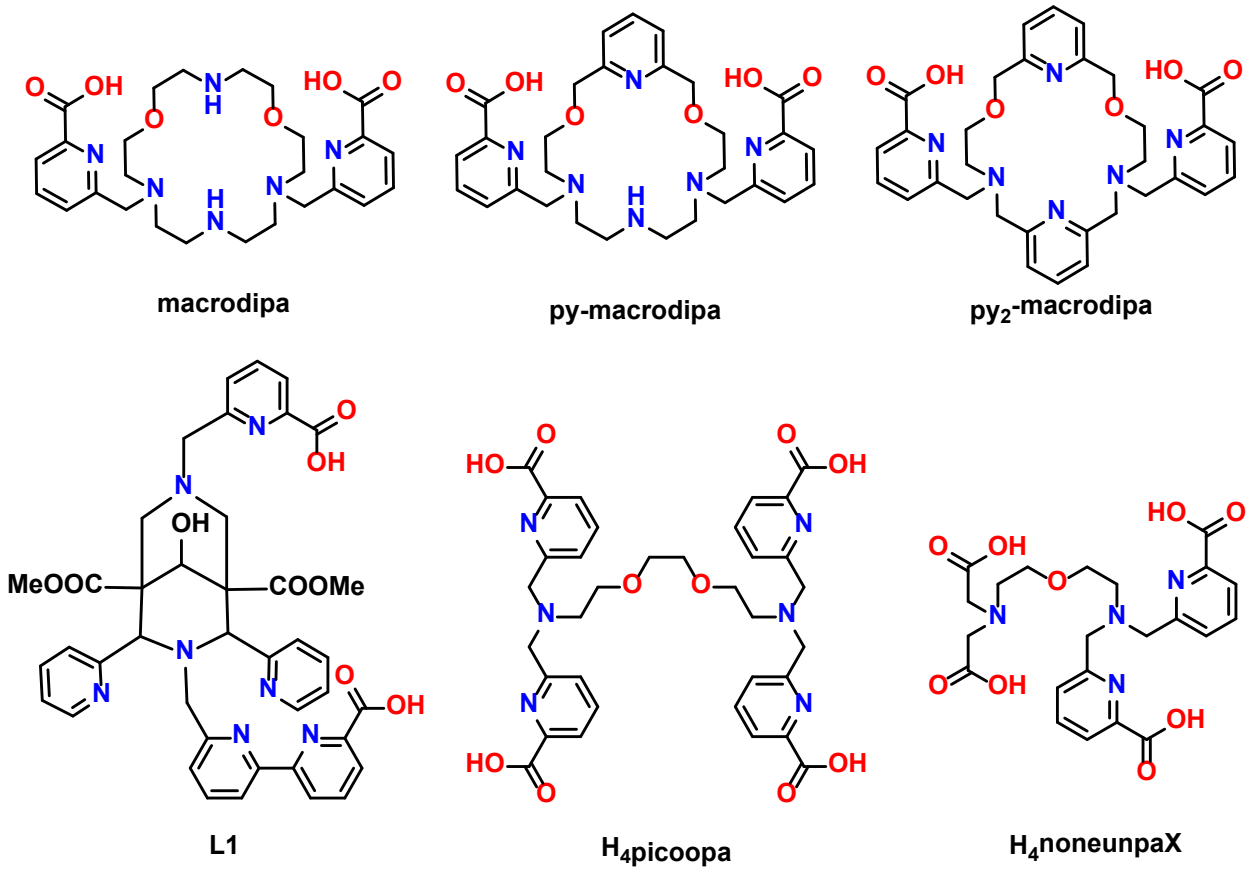

Figure S1. Chelators mentioned in the main text.

Table S1. Summary of selected structural parameters for $[La(H_2PYTA)](NO_3)\cdot 3H_2O$ and $[Ac(H_2PYTA)](NO_3)\cdot 3H_2O$ obtained from DFT periodic structure calculations.

	$[La(H_2PYTA)](NO_3)\cdot 3H_2O$[a]	$[La(H_2PYTA)](NO_3)\cdot 3H_2O$	$[Ac(H_2PYTA)](NO_3)\cdot 3H_2O$
$M–N_{py}$	2.637(1)	2.639	2.677
$M–N_{amine}$	2.702(10)	2.746	2.794
$M–O_{carb}$	2.604(69)	2.602	2.674
$N_{py}–M–N_{py}$	178.40(7)	174.94	173.57

[a]Experimental structural data were taken from single-crystal X-ray diffraction.[4] Values in parentheses are one standard deviation (of the last significant figures) from the average of crystallographically independent values.

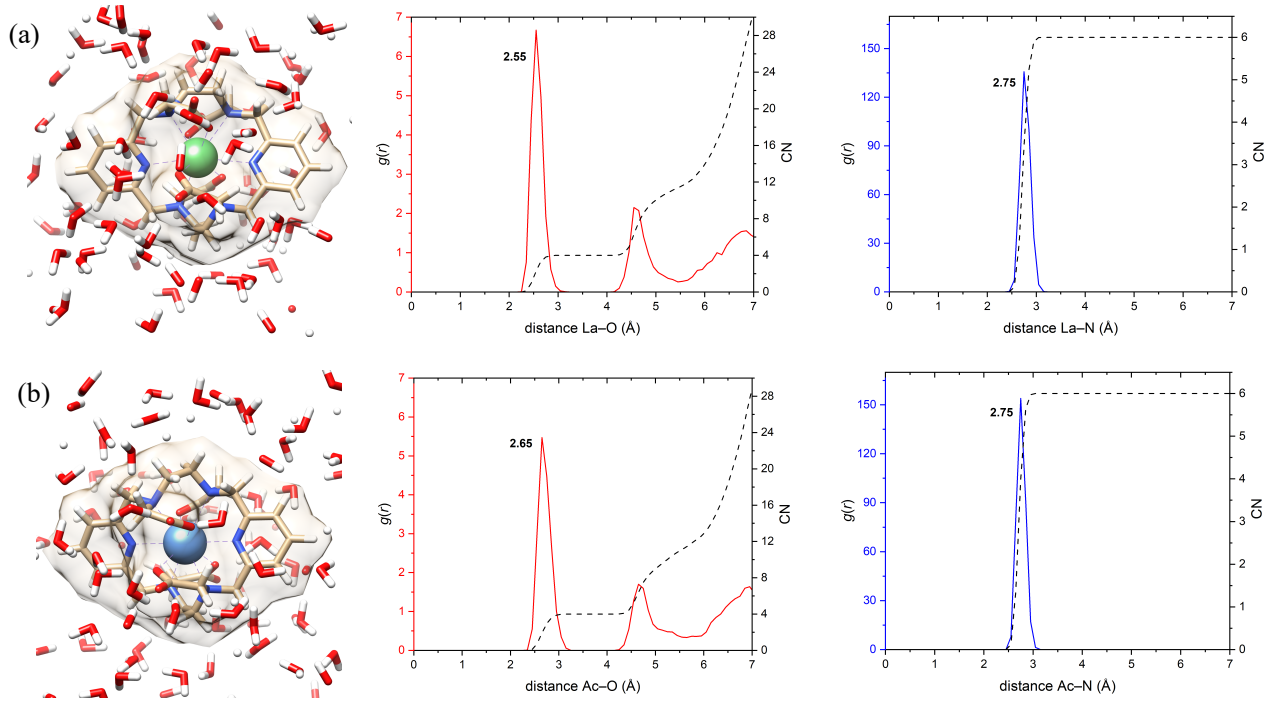

Figure S2. Structural parameters of the [La(PYTA)]$^-$ and [Ac(PYTA)]$^-$ complexes in aqueous solution obtained from ab initio molecular dynamics (AIMD) simulations. Radial distribution functions ($g(r)$; solid curve, left axis) and their integration (coordination number, CN; dashed curve, right axis) of oxygen atoms, including PYTA donor atoms and water molecules, and PYTA nitrogen atoms around (a) La^{3+} and (b) Ac^{3+}. The first peak in the La–O/Ac–O $g(r)$ originates from the interactions between La^{3+}/Ac^{3+} and carboxylate oxygens, whereas the second and third peaks correspond to atomic pair correlations with non-coordinating carboxylate oxygens and water molecules, respectively. As expected based on the larger ionic radius of Ac^{3+} versus La^{3+}, the AIMD simulations predicted a slightly longer average Ac–O bond length of 2.65 Å in comparison to the average La–O distance (2.55 Å). Notably, all four carboxylate groups remain coordinated to the metal center over the course of 20 ps, supporting the notion that the La^{3+} complex approximates the Ac^{3+} complex in solution.

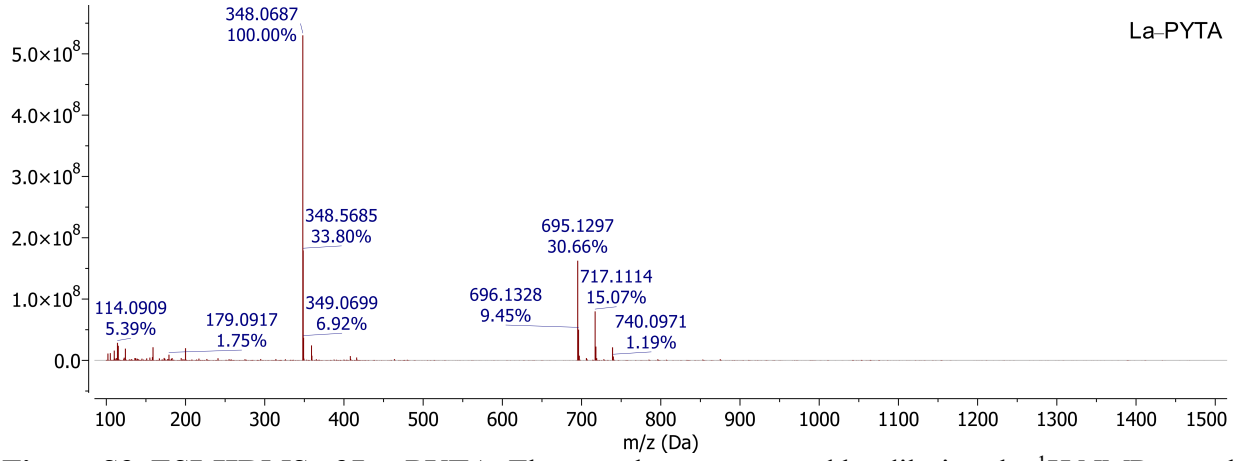

Figure S3. ESI-HRMS of La–PYTA. The sample was prepared by diluting the ^{1}H NMR sample with CH_3CN/water/formic acid (75/25/0.1). $[M+3H]^{2+}$ (*m/z* 348.0687, calcd for $[C_{26}H_{30}N_6O_8La+3H]^{2+}$: 348.0706), $[M+2H]^+$ (*m/z* 695.1297, calcd for $[C_{26}H_{30}N_6O_8La+2H]^+$: 695.1340), $[M+H+Na]^+$ (*m/z* 717.1114, calcd for $[C_{26}H_{30}N_6O_8La+H+Na]^+$: 717.1160).

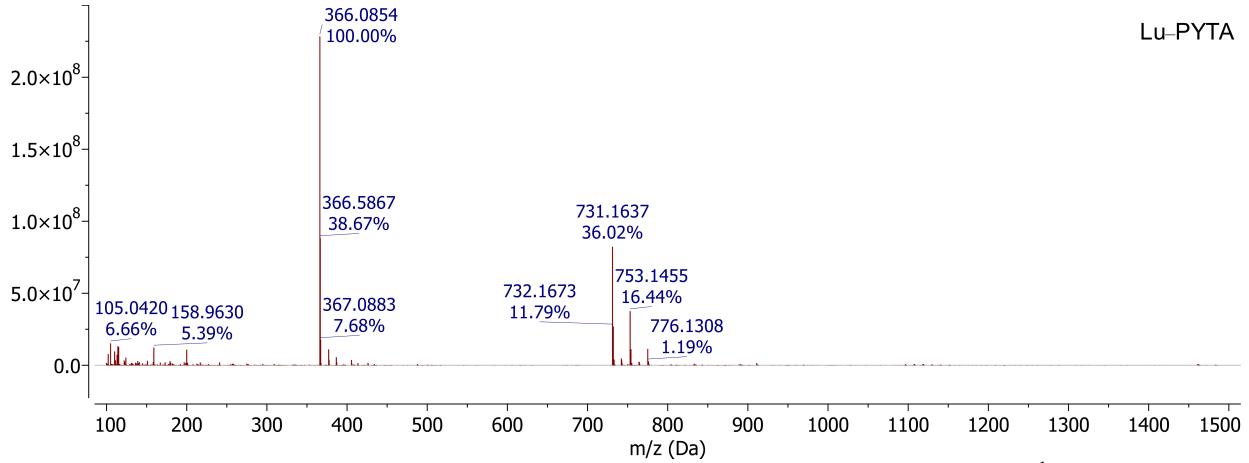

Figure S4. ESI-HRMS of Lu–PYTA. The sample was prepared by diluting the ^{1}H NMR sample with CH_3CN/water/formic acid (75/25/0.1). $[M+3H]^{2+}$ (*m/z* 366.0854, calcd for $[C_{26}H_{30}N_6O_8Lu+3H]^{2+}$: 366.0879), $[M+2H]^+$ (*m/z* 731.1637, calcd for $[C_{26}H_{30}N_6O_8Lu+2H]^+$: 731.1684), $[M+H+Na]^+$ (*m/z* 753.1455, calcd for $[C_{26}H_{30}N_6O_8Lu+H+Na]^+$: 753.1504).

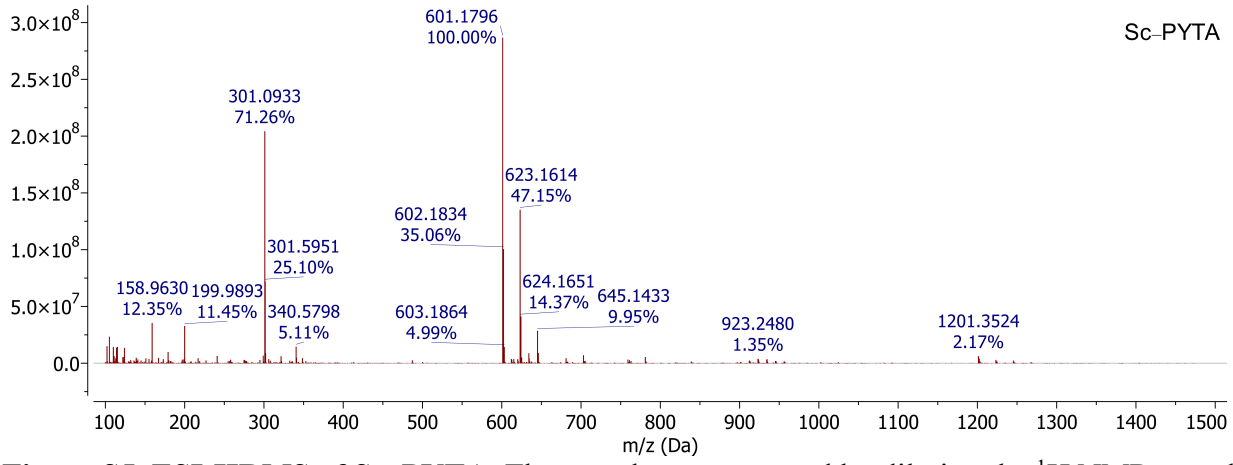

Figure S5. ESI-HRMS of Sc–PYTA. The sample was prepared by diluting the ^{1}H NMR sample with CH_3CN/water/formic acid (75/25/0.1). $[M+3H]^{2+}$ (*m/z* 301.0933, calcd for $[C_{26}H_{30}N_6O_8Sc+3H]^{2+}$: 301.0954), $[M+2H]^+$ (*m/z* 601.1796, calcd for $[C_{26}H_{30}N_6O_8Sc+2H]^+$: 601.1836), $[M+H+Na]^+$ (*m/z* 623.1614, calcd for $[C_{26}H_{30}N_6O_8Sc+H+Na]^+$: 623.1655), $[M+2Na]^+$ (*m/z* 645.1433, calcd for $[C_{26}H_{30}N_6O_8Sc+2Na]^+$: 645.1475).

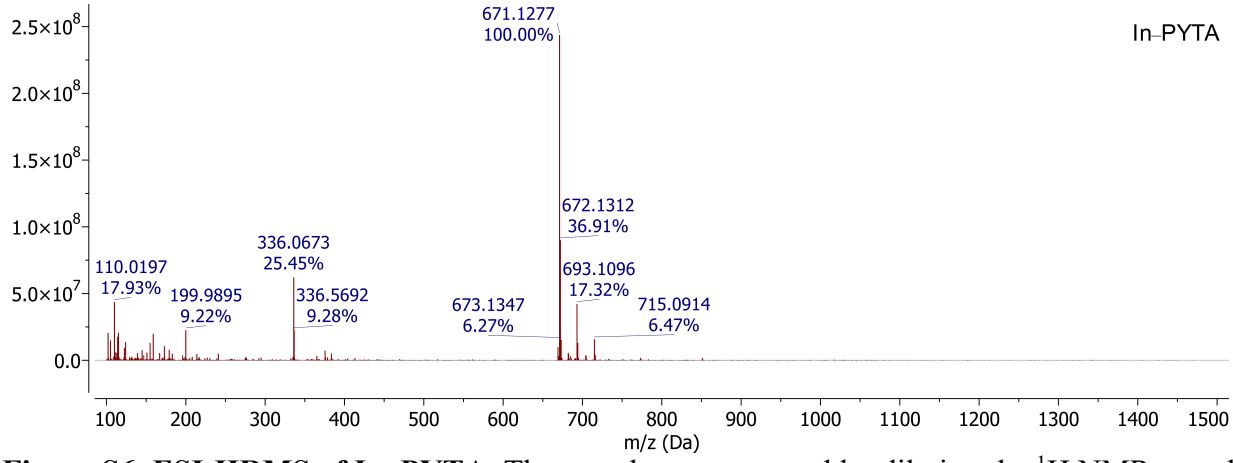

Figure S6. ESI-HRMS of In–PYTA. The sample was prepared by diluting the ^{1}H NMR sample with CH_3CN/water/formic acid (75/25/0.1). $[M+3H]^{2+}$ (*m/z* 336.0673, calcd for $[C_{26}H_{30}N_6O_8In+3H]^{2+}$: 336.0694), $[M+2H]^+$ (*m/z* 671.1277, calcd for $[C_{26}H_{30}N_6O_8In+2H]^+$: 671.1315), $[M+H+Na]^+$ (*m/z* 693.1096, calcd for $[C_{26}H_{30}N_6O_8In+H+Na]^+$: 693.1135), $[M+2Na]^+$ (*m/z* 715.0914, calcd for $[C_{26}H_{30}N_6O_8In+2Na]^+$: 715.0954).

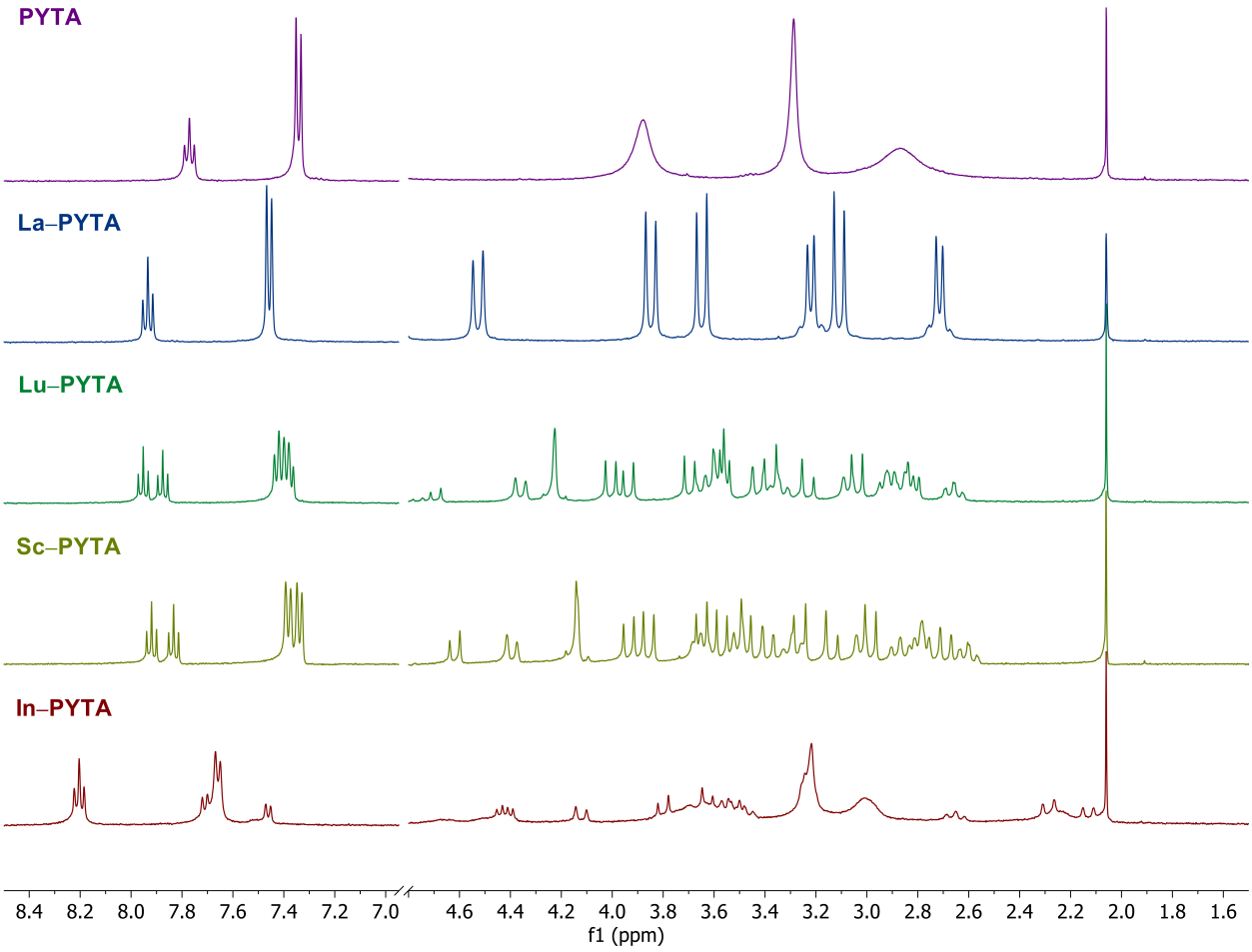

Figure S7. ^{1}H NMR spectra of metal–PYTA complexes. Top to bottom: PYTA, La–PYTA, Lu–PYTA, Sc–PYTA, and In–PYTA. 2 mM in D_2O at pD 7.0, internally referenced to acetonitrile, with suppression of H_2O via presaturation. The region between 4.6 ppm and 7.0 ppm, which contained only the residual H_2O peak, has been omitted for clarity.

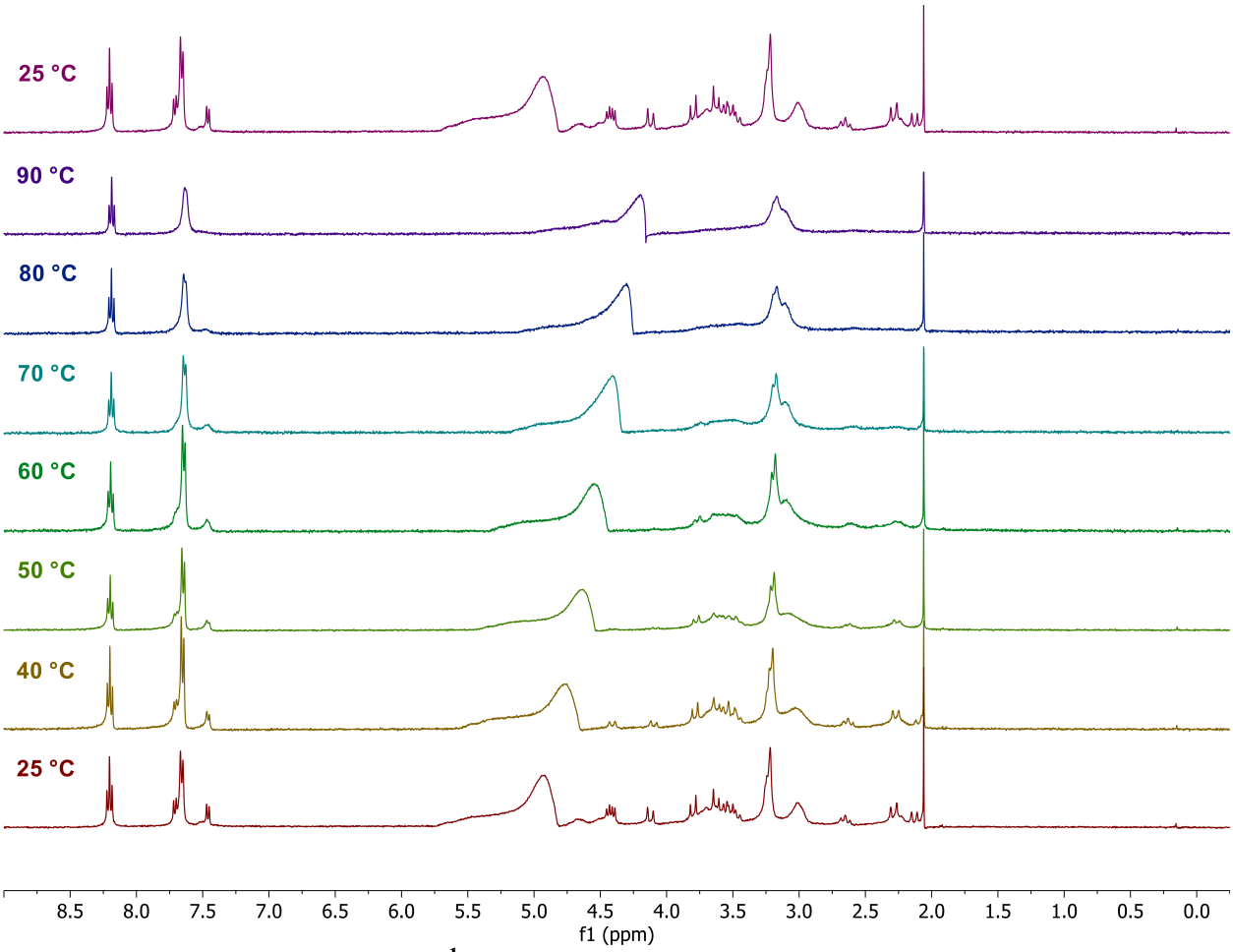

Figure S8. Variable temperature ^{1}H NMR spectra of In–PYTA. Bottom to top: 25, 40, 50, 60, 70, 80, 90, 25 °C. 2 mM in D_2O at pD 7, internally referenced to acetonitrile, with suppression of H_2O via presaturation.

Table S2. X-ray crystallographic data collection and refinement parameters for $[In(H_2PYTA)]ClO_4$, $[Sc(HPYTA)]\cdot 3H_2O$, and $[Cu(H_2PYTA)]\cdot 4H_2O$.

Compound	$[In(H_2PYTA)]ClO_4$	$[Sc(HPYTA)]\cdot 3H_2O$	$[Cu(H_2PYTA)]\cdot 4H_2O$
Empirical formula	$C_{26}H_{32}ClInN_6O_{12}$	$C_{26}H_{37}ScN_6O_{11}$	$C_{26}H_{40}CuN_6O_{12}$
Formula weight	770.84	654.57	692.18
a (Å)	30.4838(4)	37.2521(6)	13.012(5)
b (Å)	30.4838(4)	11.0181(2)	14.323(5)
c (Å)	17.4815(3)	14.5531(2)	15.919(6)
α (°)	90	90	90
β (°)	90	90.1060(10)	99.63(2)
γ (°)	120	90	90
V (Å^3)	14068.5(4)	5973.27(17)	2925.0(19)
Z	18	8	4
Crystal system	Trigonal	Monoclinic	Monoclinic
Space group	$R\bar{3}c$	$C2/c$	$C2/c$
ρ_{calc} (g/cm^3)	1.638	1.456	1.572
μ (mm^{-1})	0.913	0.316	0.822
T (K)	301.20	300.40	300.80
2*θ* range (°)	5.590 to 65.34	4.760 to 64.10	4.70 to 69.94
Independent reflections	9934	9901	6606
R_{int}	0.0251	0.0444	0.0366
Number of parameters	235	445	226
Max, min peaks (e·Å^{-3})	0.443, 0.271	0.934, 0.262	0.437, 0.349
R1[a]/wR2[b] (all data)	0.0315/0.0655	0.0529/0.1234	0.0461/0.0985
R1[a]/wR2[b] (>2σ)	0.0251/0.0617	0.0444/0.1172	0.0366/0.0928
Goodness of fit[c]	1.039	1.039	1.031

[a] $R_1 = \Sigma||Fo| - |Fc||/\Sigma|Fo|$ for $I > 2\sigma$. [b] $wR_2 = \{\Sigma[w(F_o^2 - F_c^2)^2]/\Sigma[w(F_o^2)^2]\}^{1/2}$ for $I > 2\sigma$. [c] $GoF = \{\Sigma[w(F_o^2 - F_c^2)^2]/(n - p)\}^{1/2}$, where *n* is the number of data and *p* is the number of refined parameters.

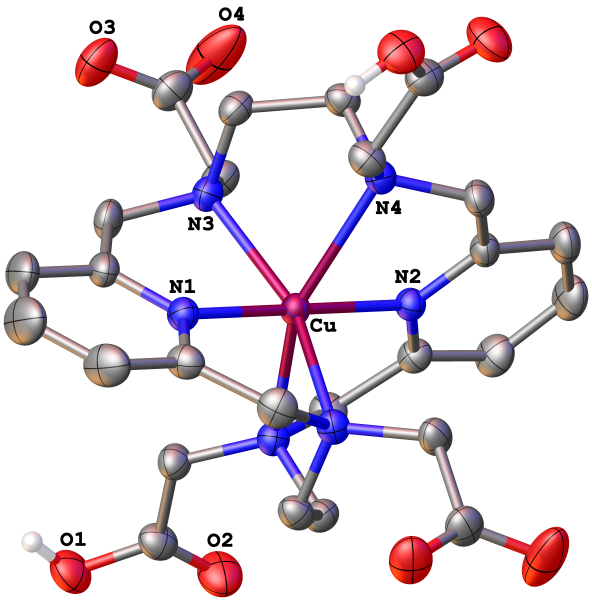

Figure S9. X-ray crystal structure of the Cu^{2+} complex of PYTA. Ellipsoids for carbons and heteroatoms are drawn at the 50% probability level. Outer-sphere solvent molecules and hydrogen atoms attached to carbon centers have been omitted for clarity.

Table S3. TLC systems and retention factors (R_f) for radiolabeling experiments of PYTA, macropa, and DOTA with $^{225}Ac^{3+}$, $[^{177}Lu]Lu^{3+}$, $[^{111}In]In^{3+}$, and $[^{44}Sc]Sc^{3+}$.

	$^{225}Ac^{3+}$			**$[^{177}Lu]Lu^{3+}$**			**$[^{111}In]In^{3+}$**			**$[^{44}Sc]Sc^{3+}$**		
	TLC	R_f M^{3+}	R_f M–L	TLC	R_f M^{3+}	R_f M–L	TLC	R_f M^{3+}	R_f M–L	TLC	R_f M^{3+}	R_f M–L
PYTA	A or B	1	0.04	B	1	0.04	B	0.8-1	0.06	C	0.2	0.4
macropa	A	1	0.08	A	1	0.06	B	0.8-1	0.01	D	0.9	0.2
DOTA	B	1	0.12	B	1	0.12	B	0.8-1	0.09	E	0.2	0.8

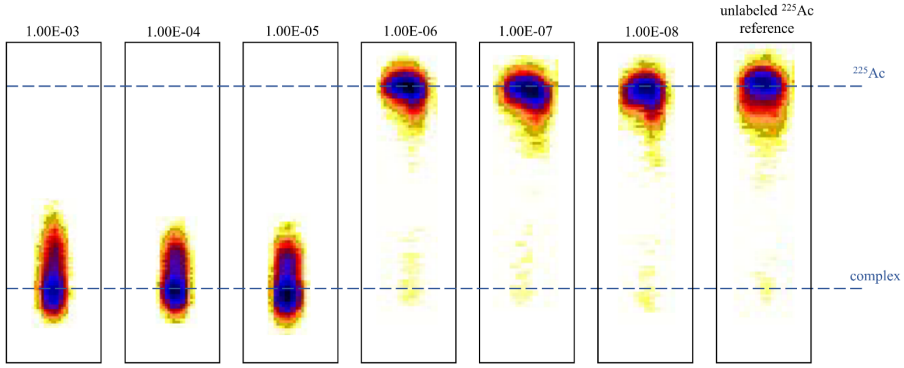

Figure S10. Representative radio-TLC traces from $^{225}Ac^{3+}$ radiolabeling of PYTA using TLC system A. Reaction conditions: NH_4OAc buffer (0.5 M, pH 6), RT, 5 min, 9.3–11.1 kBq of ^{225}Ac, 10^{-8} –10^{-3} M PYTA, V_{tot} = 150 µL.

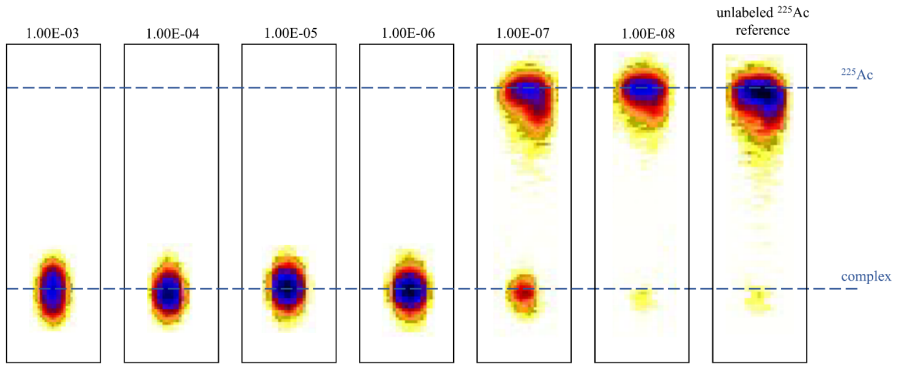

Figure S11. Representative radio-TLC traces from $^{225}Ac^{3+}$ radiolabeling of macropa using TLC system A. Reaction conditions: NH_4OAc buffer (0.5 M, pH 6), RT, 5 min, 9.3–11.1 kBq of ^{225}Ac, 10^{-8} –10^{-3} M macropa, V_{tot} = 150 µL. Figure reproduced from ref 20.

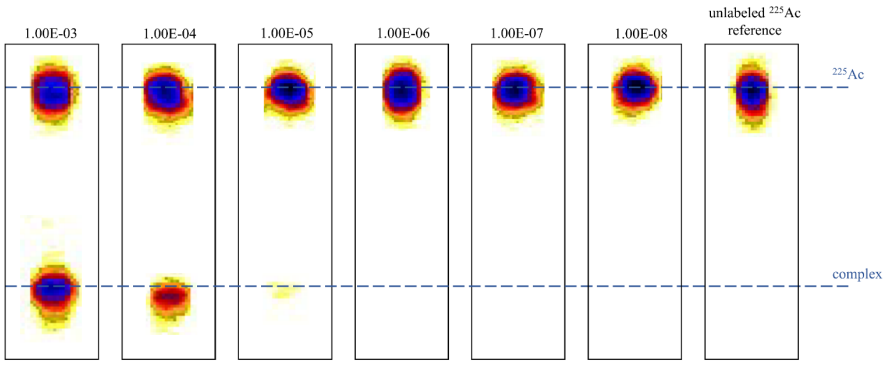

Figure S12. Representative radio-TLC traces from $^{225}Ac^{3+}$ radiolabeling of <u>DOTA</u> using TLC system B. Reaction conditions: NH_4OAc buffer (0.5 M, pH 6), RT, 5 min, 9.3–11.1 kBq of ^{225}Ac, 10^{-8} –10^{-3} M DOTA, V_{tot} = 150 µL.

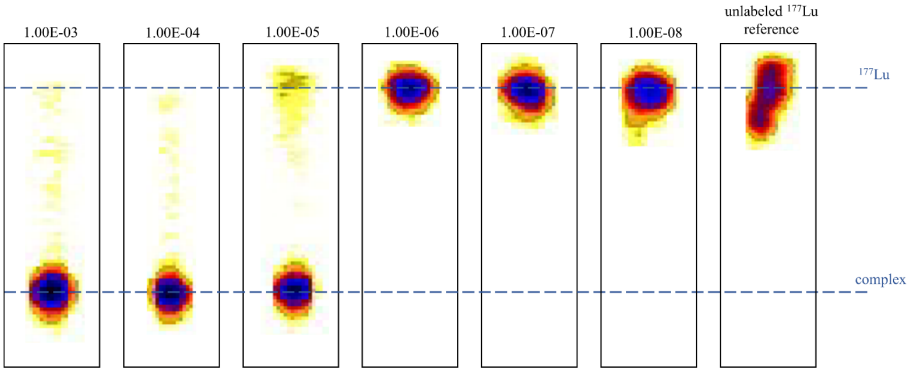

Figure S13. Representative radio-TLC traces from $[^{177}Lu]Lu^{3+}$ radiolabeling of <u>PYTA</u> using TLC system B. Reaction conditions: NH_4OAc buffer (0.5 M, pH 6), RT, 5 min, 22–37 kBq of ^{177}Lu, 10^{-8} –10^{-3} M PYTA, V_{tot} = 150 µL.

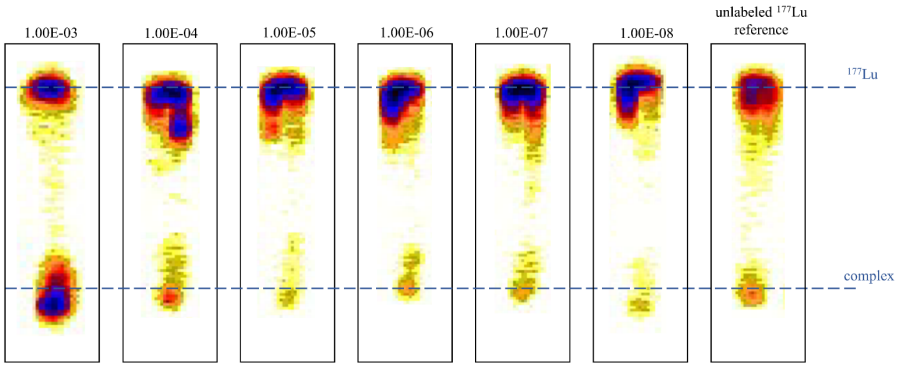

Figure S14. Representative radio-TLC traces from $[^{177}Lu]Lu^{3+}$ radiolabeling of <u>macropa</u> using TLC system A. Reaction conditions: NH_4OAc buffer (0.5 M, pH 6), RT, 5 min, 22–37 kBq of ^{177}Lu, 10^{-8} –10^{-3} M macropa, V_{tot} = 150 µL.

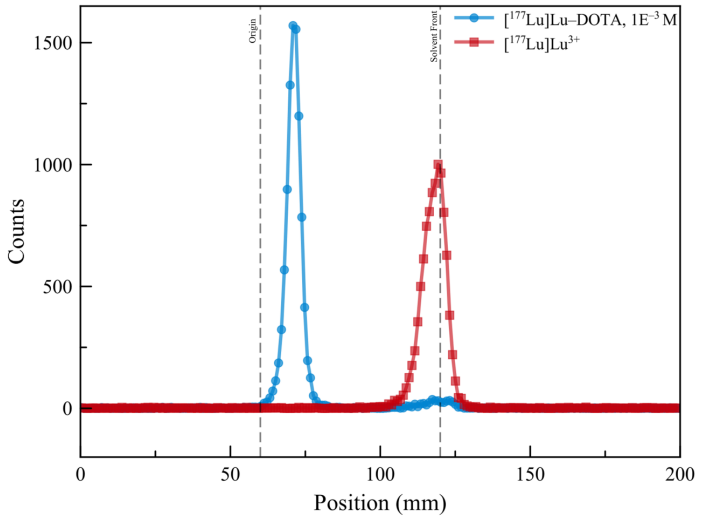

Figure S15. Representative radio-TLC traces from [^{177}Lu]Lu^{3+} radiolabeling of <u>DOTA</u> using TLC system B. Reaction conditions: NH_4OAc buffer (0.5 M, pH 6), RT, 5 min, 22–37 kBq of ^{177}Lu, 1 × 10^{-3} M DOTA, V_{tot} = 150 µL.

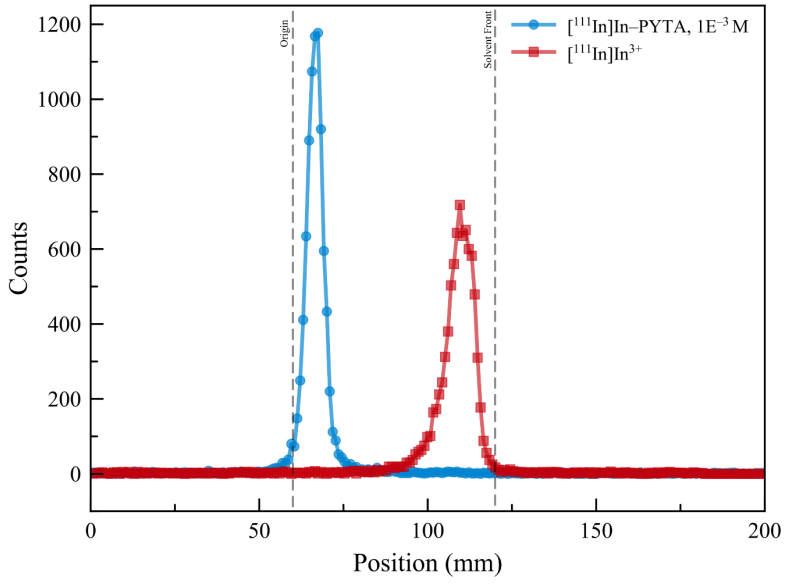

Figure S16. Representative radio-TLC traces from [^{111}In]In^{3+} radiolabeling of <u>PYTA</u> using TLC system B. Reaction conditions: NH_4OAc buffer (0.5 M, pH 6), RT, 5 min, 74–111 kBq of ^{111}In, 1 × 10^{-3} M PYTA, V_{tot} = 150 µL.

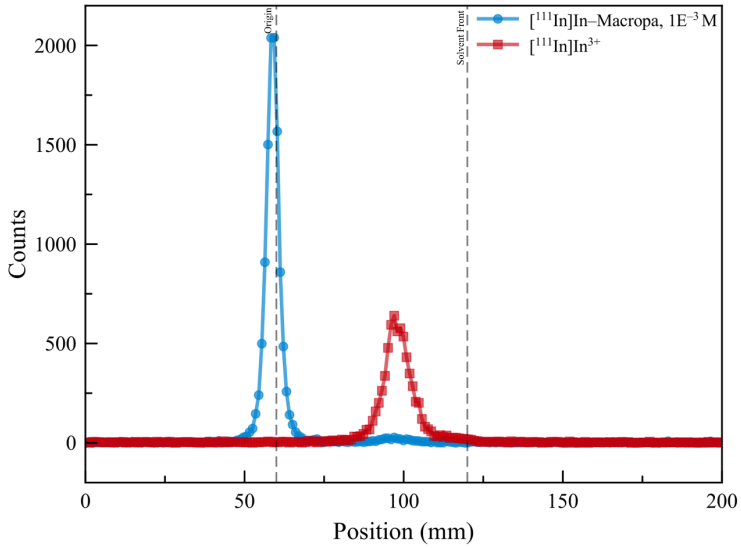

Figure S17. Representative radio-TLC traces from [^{111}In]In^{3+} radiolabeling of <u>macropa</u> using TLC system B. Reaction conditions: NH_4OAc buffer (0.5 M, pH 6), RT, 5 min, 74–111 kBq of ^{111}In, 1×10^{-3} M macropa, V_{tot} = 150 µL.

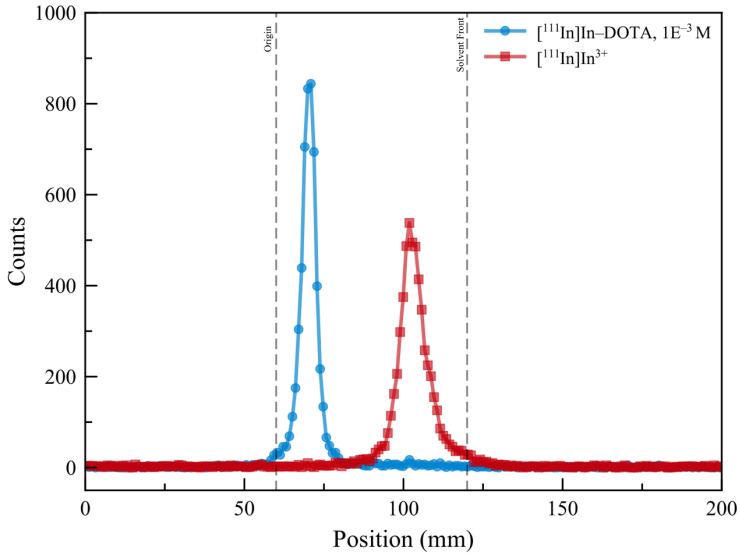

Figure S18. Representative radio-TLC traces from [^{111}In]In^{3+} radiolabeling of <u>DOTA</u> using TLC system B. Reaction conditions: NH_4OAc buffer (0.5 M, pH 6), RT, 5 min, 74–111 kBq of ^{111}In, 1×10^{-3} M DOTA, V_{tot} = 150 µL.

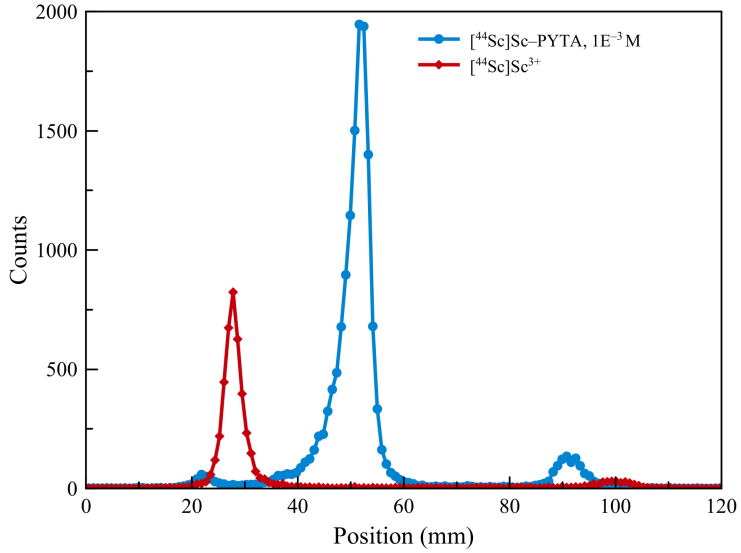

Figure S19. Representative radio-TLC traces from [^{44}Sc]Sc^{3+} radiolabeling with <u>PYTA</u> using TLC system C. Reaction conditions: NH_4OAc buffer (0.5 M, **pH 6**), RT, 5 min, 185 KBq of ^{44}Sc, 1 × 10^{-3} M PYTA, V_{tot} = 150 µL.

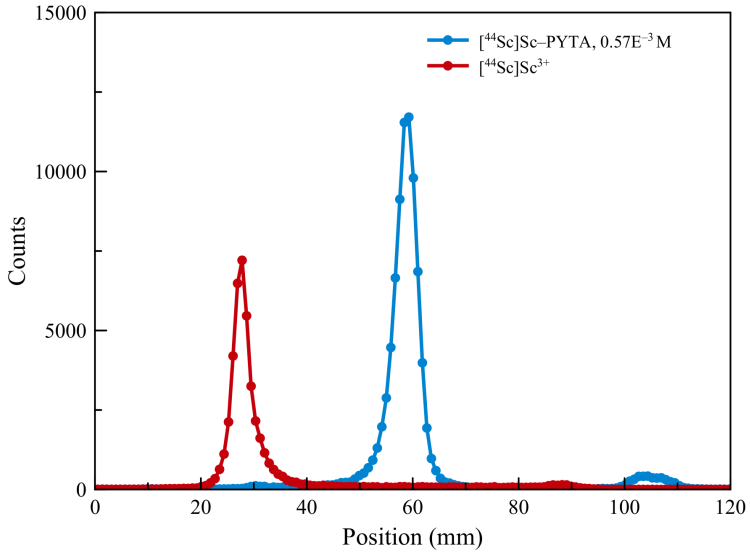

Figure S20. Representative radio-TLC traces from [^{44}Sc]Sc^{3+} radiolabeling with <u>PYTA</u> using TLC system C. Reaction conditions: NH_4OAc buffer (0.25 M, **pH 4.05**), RT, 30 min, 1.665 MBq of ^{44}Sc, 0.57 × 10^{-3} M PYTA, V_{tot} = 100 µL.

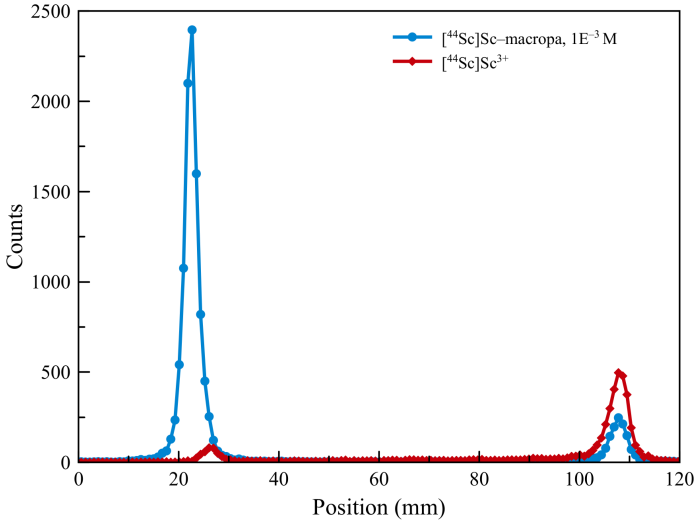

Figure S21. Representative radio-TLC traces from $[^{44}Sc]Sc^{3+}$ radiolabeling with <u>macropa</u> using TLC system D. Reaction conditions: NH_4OAc buffer (0.5 M, pH 6), RT, 5 min, 185 kBq of ^{44}Sc, 1×10^{-3} M macropa, V_{tot} = 150 µL.

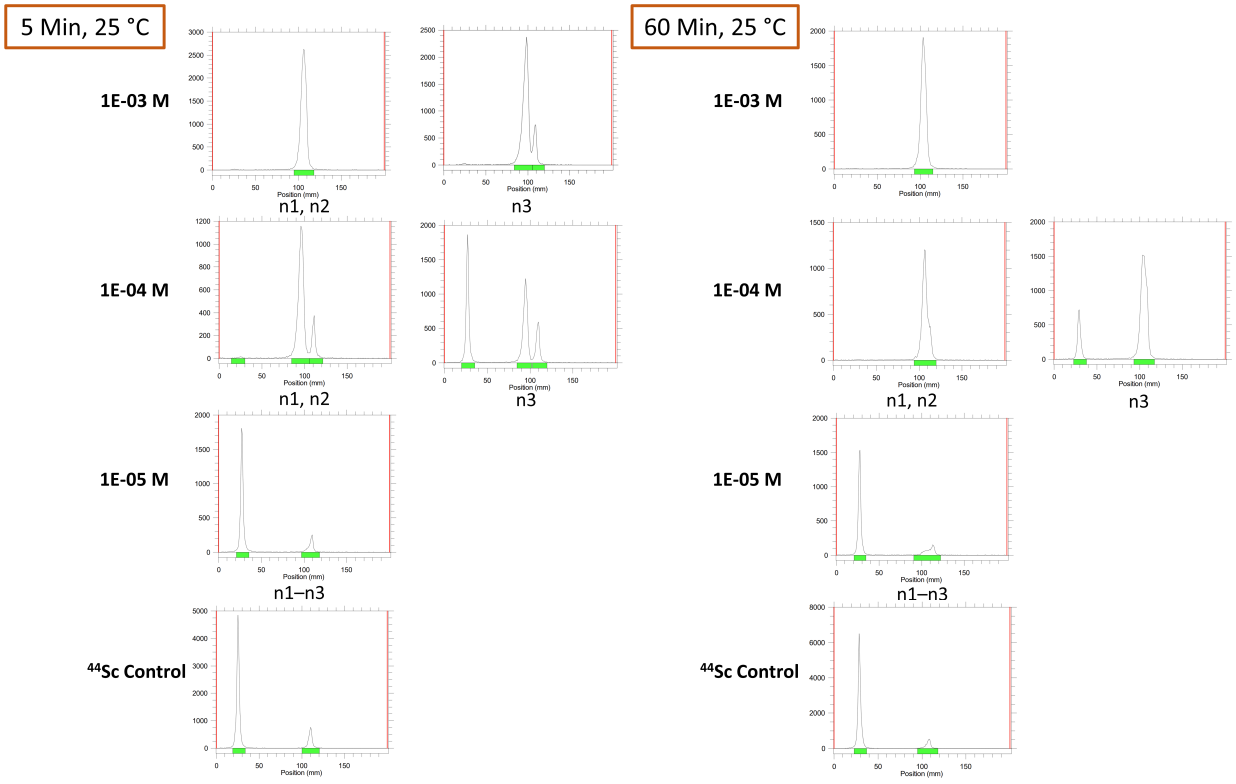

Figure S22. Representative radio-TLC traces from $[^{44}Sc]Sc^{3+}$ radiolabeling with <u>DOTA</u> (various concentrations) using TLC system E. Reaction conditions: NH_4OAc buffer (0.5 M, pH 6), **RT**, 5 or 60 min, 185 kBq of ^{44}Sc, V_{tot} = 150 µL. At RT, even after 60 min, DOTA shows inconsistent radiolabeling. By contrast, we did not observe this variability for radiolabeling reactions at 80 °C under the same conditions.

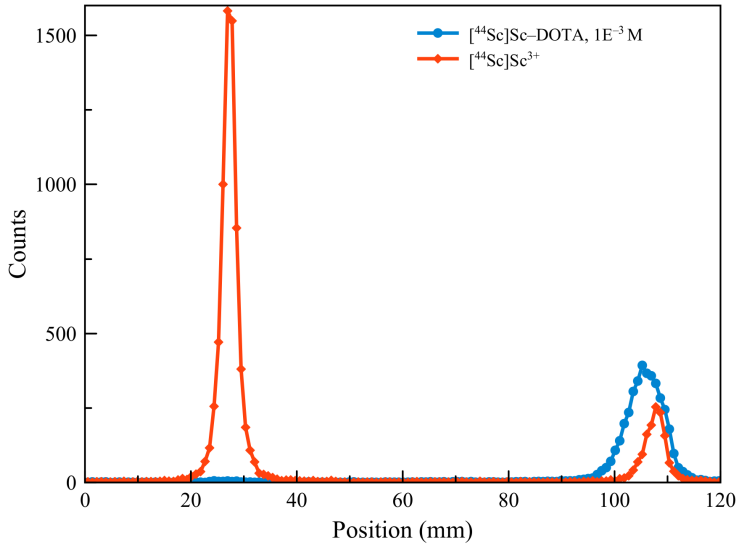

Figure S23. Representative radio-TLC traces from [^{44}Sc]Sc^{3+} radiolabeling with <u>DOTA</u> using TLC system E. Reaction conditions: NH_4OAc buffer (0.5 M, pH 6), **80 °C**, 5 min, 185 kBq of ^{44}Sc, 1×10^{-3} M DOTA, V_{tot} = 150 µL.

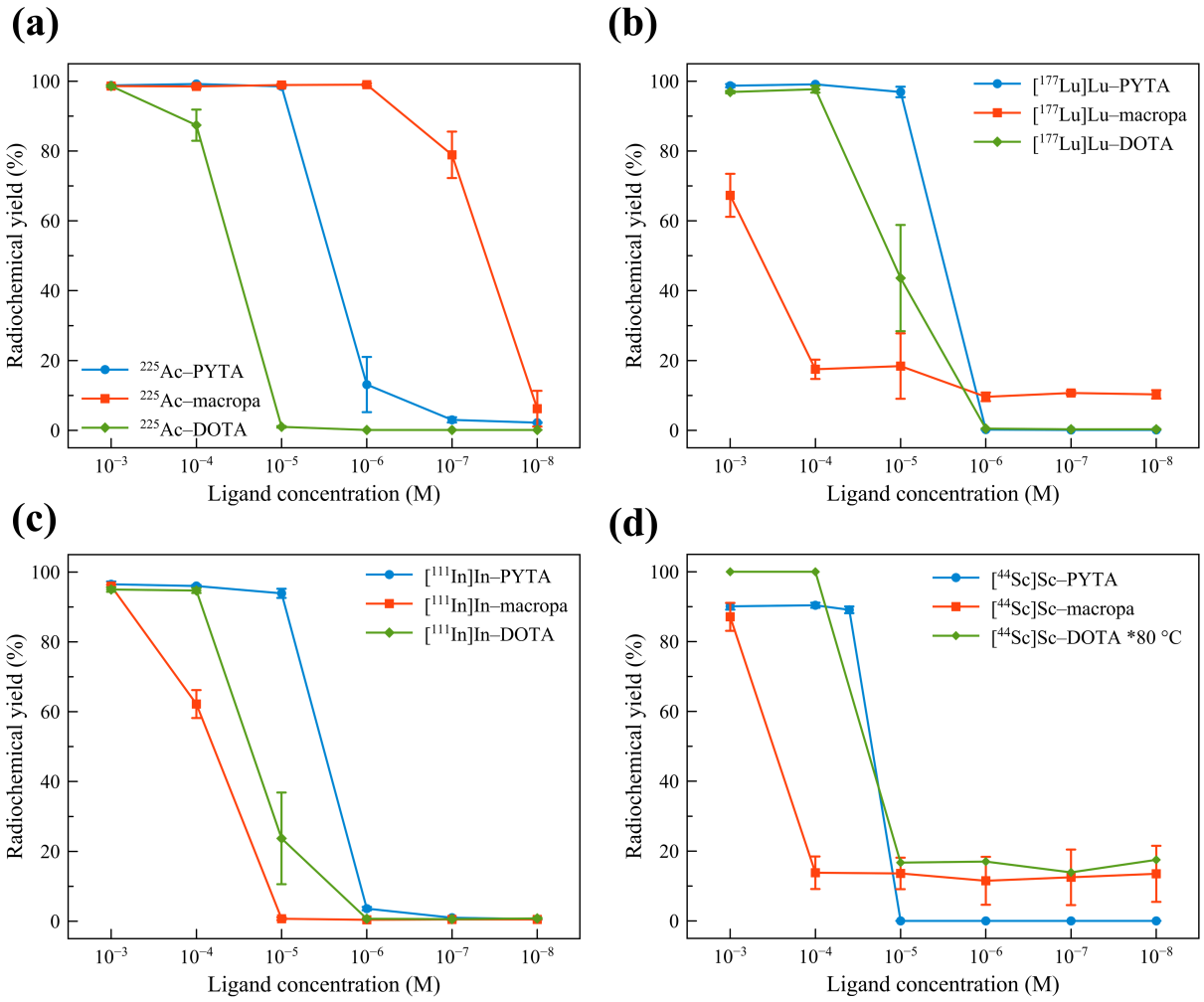

Figure S24. Concentration-dependent radiolabeling of PYTA, macropa, and DOTA with (a) $^{225}Ac^{3+}$ (9.3–11.1 kBq), (b) [^{177}Lu]Lu^{3+} (22–37 kBq), (c) [^{111}In]In^{3+} (74–111 kBq), or (d) [^{44}Sc]Sc^{3+} (185 kBq) after 60 min reaction time. All reactions were carried out at 25 °C in NH_4OAc (0.5 M, pH 6.0), V_T = 150 µL, except for the ^{44}Sc/DOTA radiolabeling, for which data from 80 °C experiments are shown. The error bars represent the standard deviations. Data for ^{225}Ac–macropa and ^{225}Ac–DOTA were reproduced from ref 20.

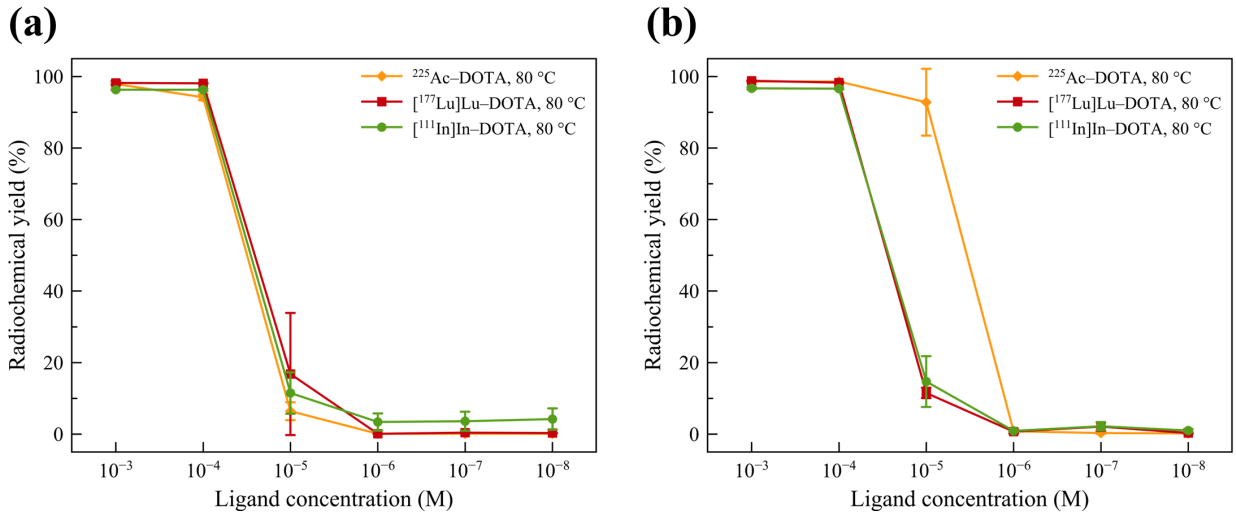

Figure S25. Concentration-dependent radiolabeling of DOTA with $^{225}Ac^{3+}$ (9.3–11.1 kBq), $[^{177}Lu]Lu^{3+}$ (22–37 kBq), and $[^{111}In]In^{3+}$ (74–111 kBq) at 80 °C after (a) 5 min or (b) 60 min reaction time. All reactions were carried out in NH_4OAc (0.5 M, pH 6.0), V_T = 150 µL. The error bars represent the standard deviations.

Table S4. TLC systems and chelator concentrations used in serum challenges.

	$^{225}Ac^{3+}$			$[^{177}Lu]Lu^{3+}$			$[^{111}In]In^{3+}$			$[^{44}Sc]Sc^{3+}$		
	TLC	[L] before serum	[L] after serum	TLC	[L] before serum	[L] after serum	TLC	[L] before serum	[L] after serum	TLC	[L] before serum	[L] after serum
PYTA	B	4×10^{-5}	1×10^{-5}	B	4×10^{-5}	1×10^{-5}	B	4×10^{-5}	1×10^{-5}	F	4×10^{-5} or 4×10^{-4}	1×10^{-5} or 1×10^{-4}
macropa	A	4×10^{-5}	1×10^{-5}	A	4×10^{-3}	1×10^{-3}	B	3.34×10^{-3} or 4×10^{-4}	8.4×10^{-4} or 1×10^{-4}	–	–	–
DOTA	B	4×10^{-5}	1×10^{-5}	B	4×10^{-4}	1×10^{-4}	B	4×10^{-4}	1×10^{-4}	–	–	–

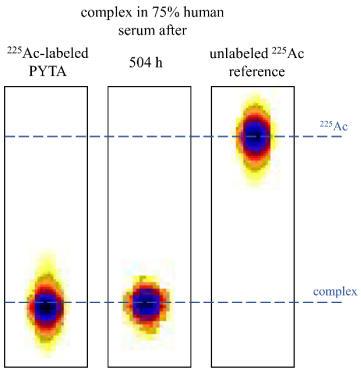

Figure S26. Representative radio-TLC traces (TLC system B) from experiments challenging ^{225}Ac–PYTA with human serum. Reaction conditions: 75% human serum, 25% NH_4OAc buffer (0.5 M, pH 6), 37 °C, 37 kBq of ^{225}Ac, V_{tot} = 600 µL.

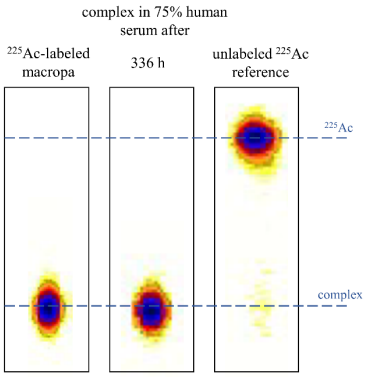

Figure S27. Representative radio-TLC traces (TLC system A) from experiments challenging ^{225}Ac–macropa with human serum. Reaction conditions: 75% human serum, 25% NH_4OAc buffer (0.5 M, pH 6), 37 °C, 37 kBq of ^{225}Ac, V_{tot} = 600 µL. Figure taken from ref 20.

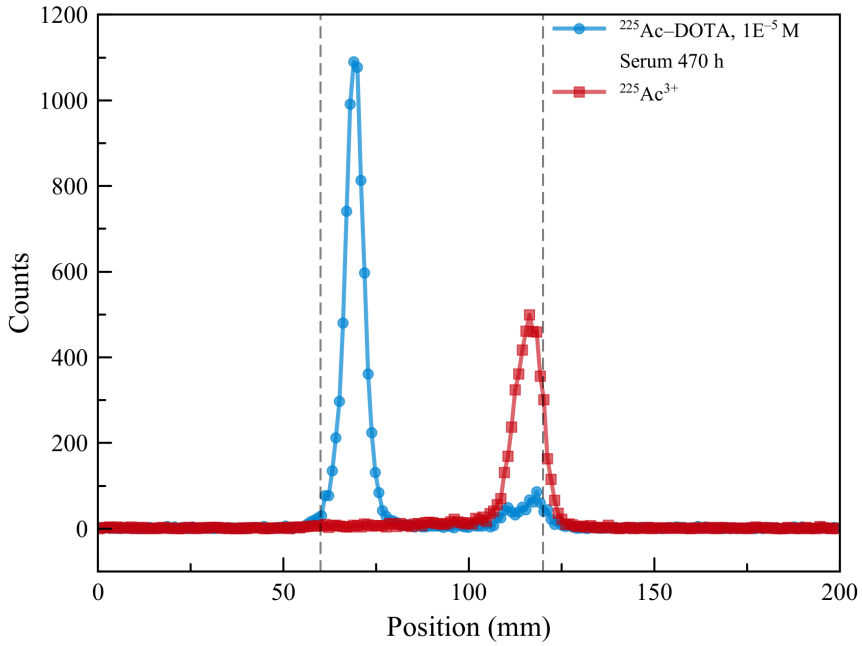

Figure S28. Representative radio-TLC traces (TLC system B) from experiments challenging ^{225}Ac–DOTA with human serum. Reaction conditions: 75% human serum, 25% NH_4OAc buffer (0.5 M, pH 6), 37 °C, 37 kBq of ^{225}Ac, V_{tot} = 600 µL.

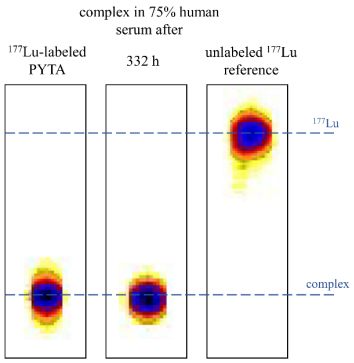

Figure S29. Representative radio-TLC traces (TLC system B) from experiments challenging [^{177}Lu]Lu–PYTA with human serum. Reaction conditions: 75% human serum, 25% NH_4OAc buffer (0.5 M, pH 6), 37 °C, 148 kBq of ^{177}Lu, V_{tot} = 600 µL.

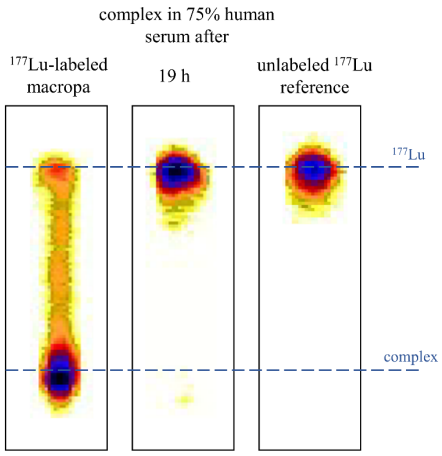

Figure S30. Representative radio-TLC traces (TLC system A) from experiments challenging [^{177}Lu]Lu–macropa with human serum. Reaction conditions: 75% human serum, 25% NH_4OAc buffer (0.5 M, pH 6), 37 °C, 148 kBq of ^{177}Lu, V_{tot} = 600 µL.

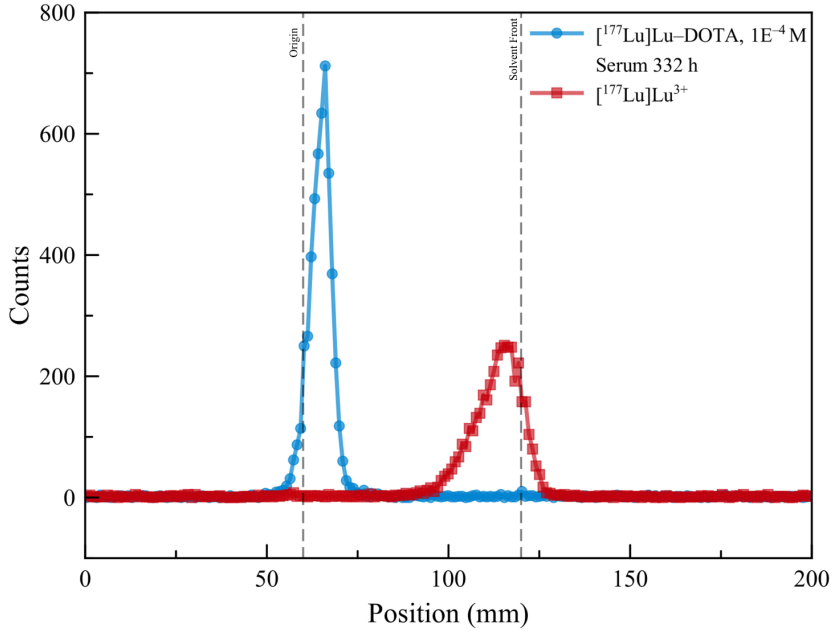

Figure S31. Representative radio-TLC traces (TLC system B) from experiments challenging [^{177}Lu]Lu–DOTA with human serum. Reaction conditions: 75% human serum, 25% NH_4OAc buffer (0.5 M, pH 6), 37 °C, 148 kBq of ^{177}Lu, V_{tot} = 600 µL.

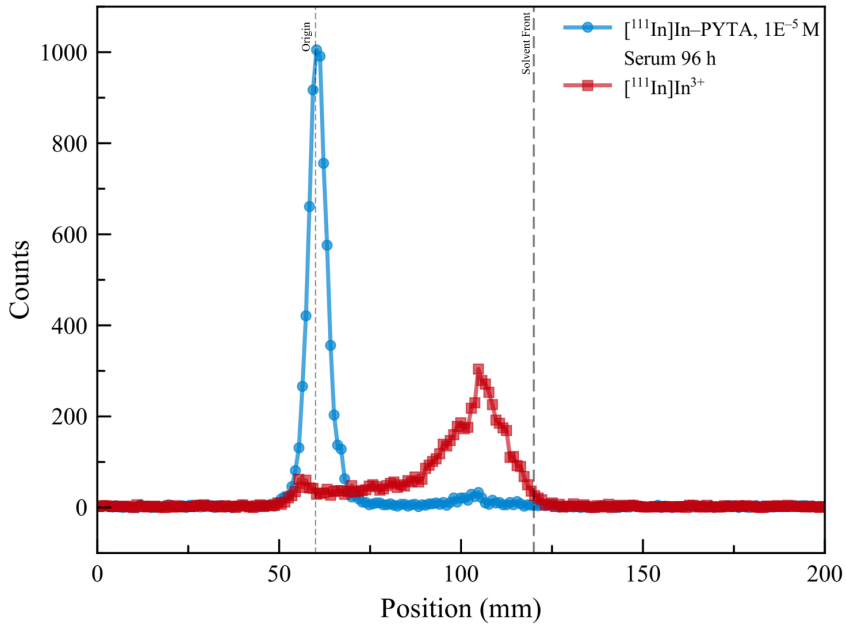

Figure S32. Representative radio-TLC traces (TLC system B) from experiments challenging [^{111}In]In–PYTA with human serum. Reaction conditions: 75% human serum, 25% NH_4OAc buffer (0.5 M, pH 6), 37 °C, 185–296 kBq of ^{111}In, V_{tot} = 600 µL.

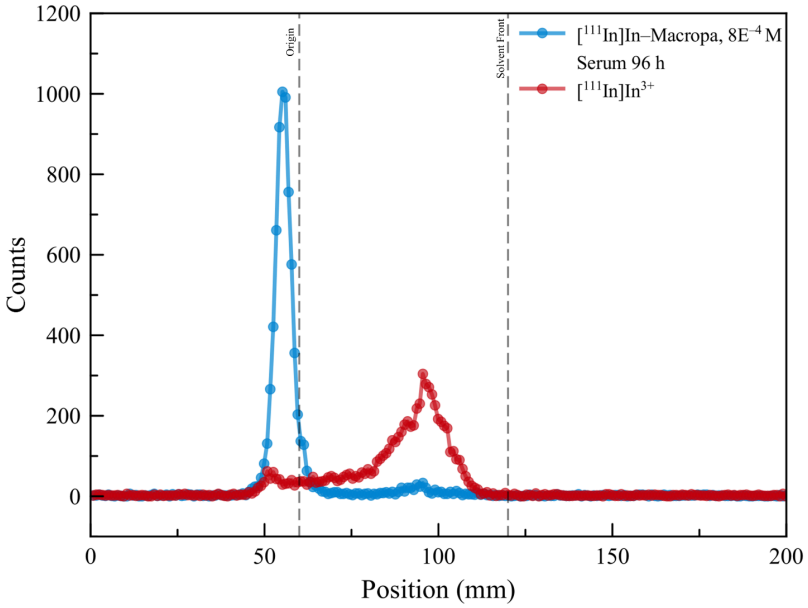

Figure S33. Representative radio-TLC traces (TLC system B) from experiments challenging [^{111}In]In–macropa with human serum. Reaction conditions: 75% human serum, 25% NH_4OAc buffer (0.5 M, pH 6), 37 °C, 185–296 kBq of ^{111}In, V_{tot} = 600 µL. Final concentration of macropa = 8.4×10^{-4} M.

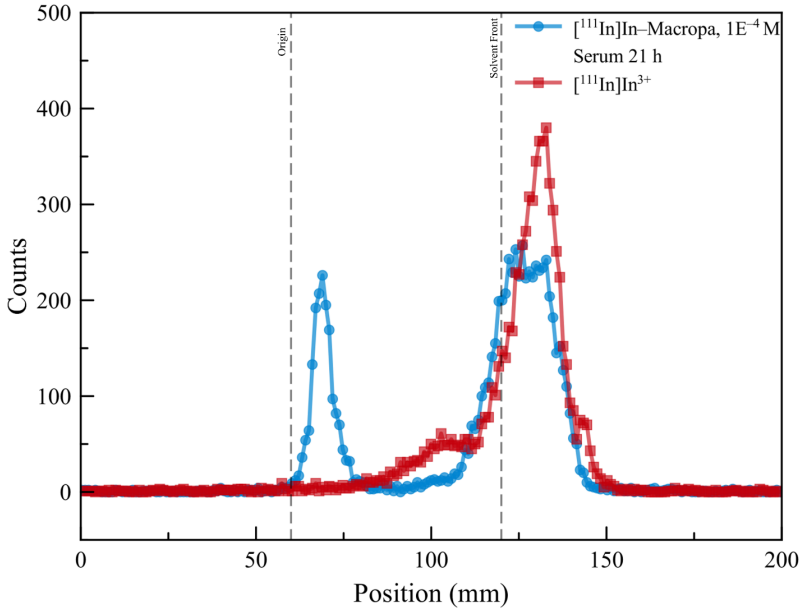

Figure S34. Representative radio-TLC traces (TLC system B) from experiments challenging [^{111}In]In–macropa with human serum. Reaction conditions: 75% human serum, 25% NH_4OAc buffer (0.5 M, pH 6), 37 °C, 185–296 kBq of ^{111}In, V_{tot} = 600 µL. Final concentration of macropa = 1×10^{-4} M.

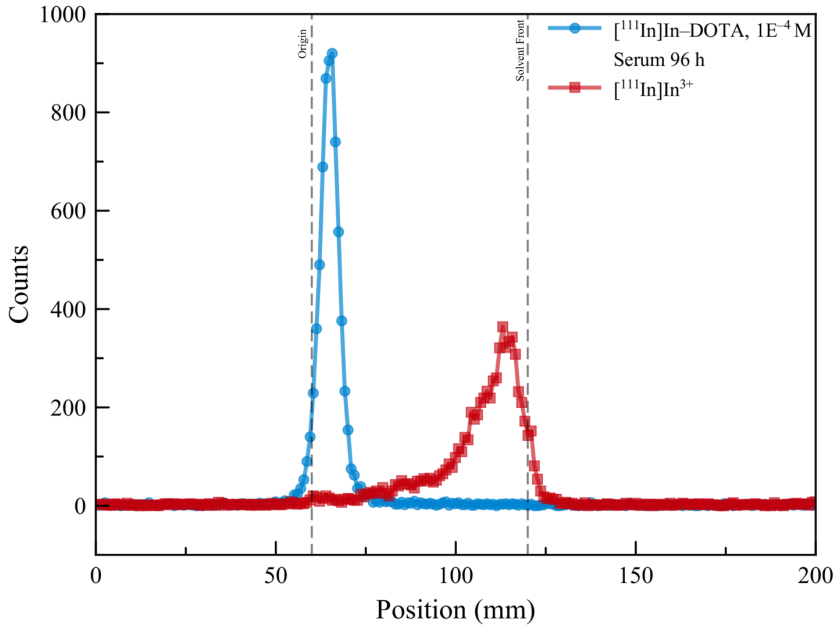

Figure S35. Representative radio-TLC traces (TLC system B) from experiments challenging [^{111}In]In–DOTA with human serum. Reaction conditions: 75% human serum, 25% NH_4OAc buffer (0.5 M, pH 6), 37 °C, 185–296 kBq of ^{111}In, V_{tot} = 600 µL.

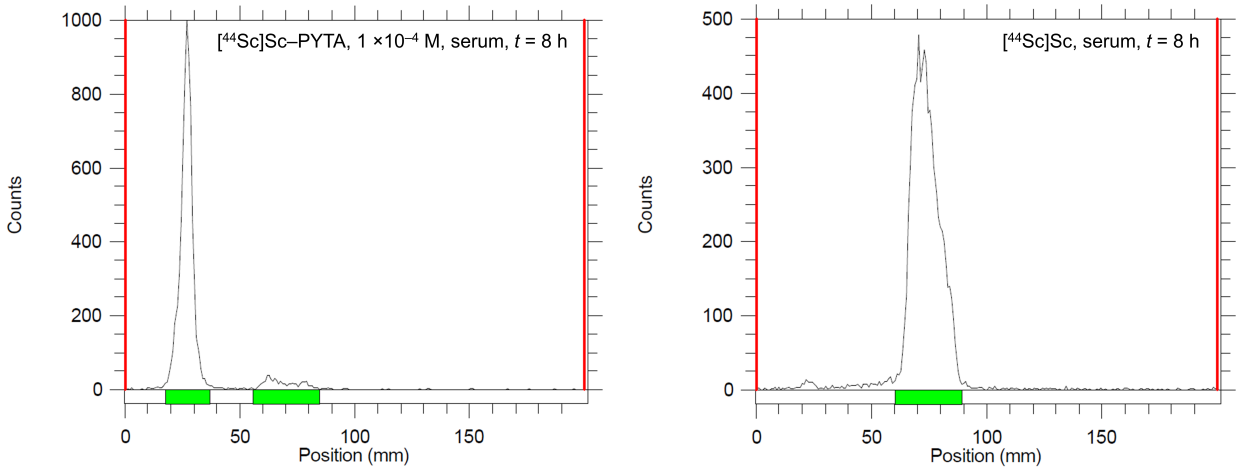

Figure S36. Representative radio-TLC traces (TLC system X) from experiments challenging [^{44}Sc]Sc–PYTA with human serum. Reaction conditions: 75% human serum, 25% NH_4OAc buffer (0.5 M, pH 6), 37 °C, 740 kBq of ^{44}Sc, V_{tot} = 600 µL. Final concentration of PYTA = 1×10^{-4} M.

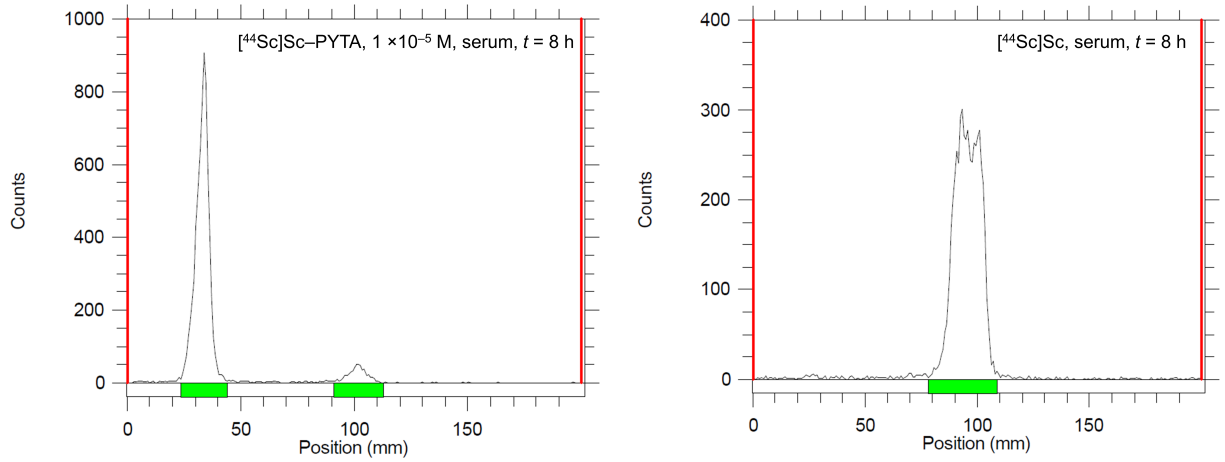

Figure S37. Representative radio-TLC traces (TLC system X) from experiments challenging [^{44}Sc]Sc–PYTA with human serum. Reaction conditions: 75% human serum, 25% NH_4OAc buffer (0.5 M, pH 6), 37 °C, 740 kBq of ^{44}Sc, V_{tot} = 600 µL. Final concentration of PYTA = 1×10^{-5} M.

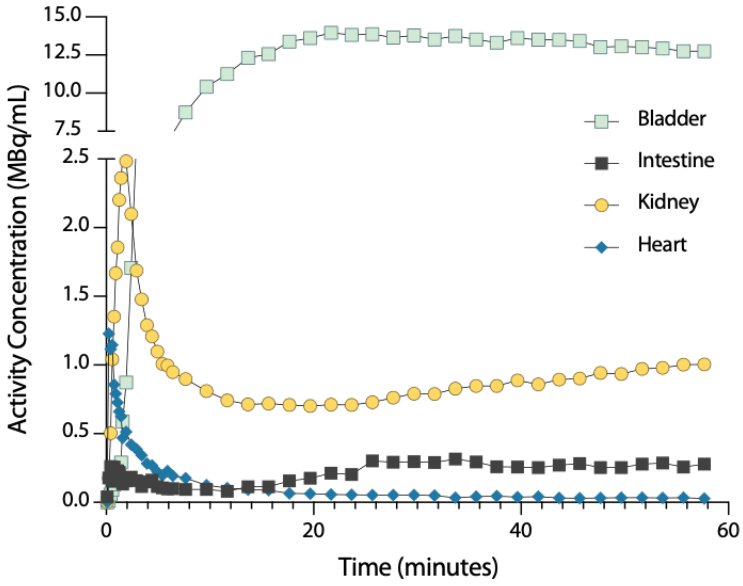

Figure S38. Volumes of interest (VOI) analysis of dynamic PET imaging of [^{44}Sc]Sc–PYTA.

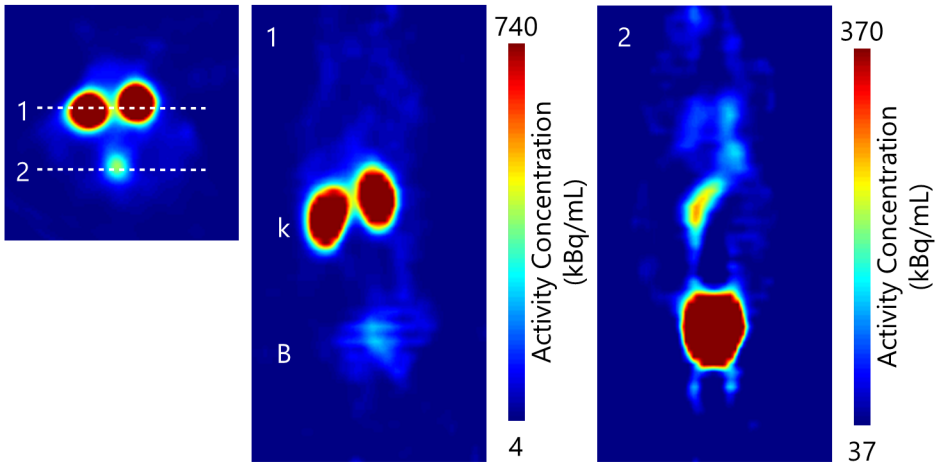

Figure S39. 2D quantitative slices of PET images of [^{44}Sc]Sc–PYTA at t = 60 min, showing (plane 1) kidney and (plane 2) gut uptake and bladder clearance.

Table S5. Organ distribution of [^{44}Sc]Sc–PYTA after intravenous injection in mice (%ID/g).

t = 15 min	n1	n2	n3	n4
Blood	3.740672	2.870511	5.447241	3.358018
Heart	1.829624	1.260428	1.542745	1.202436
Lungs	2.197085	2.417542	2.62914	2.160869
Liver	2.075453	2.104218	3.173952	2.100306
Spleen	1.011196	0.754526	1.150906	0.744143
Kidney	10.9922	7.42735	15.35408	7.591421
Stomach	0.851508	0.660415	2.018993	2.144943
Lg. Intestine	0.978884	0.769048	1.560475	1.185254
Muscle	1.19184	1.34957	0.926328	1.152549
Fat	0.372447	1.267682	0.569906	0.498061
Calvaria	2.358495	1.476982	1.756608	1.170077
Brain	0.155457	0.162442	0.276136	0.154281

t = 1 h	n1	n2	n3	n4
Blood	0.109118	0.185081	0.175089	0.155051
Heart	0.078047	0.094829	0.099297	0.0784
Lungs	0.137734	0.147641	0.208895	0.136081
Liver	0.142965	0.235978	0.143774	0.15732
Spleen	0.092164	0.08886	0.10343	0.090316
Kidney	23.21309	1.522468	1.478234	4.257172
Stomach	0.152447	0.156897	0.228015	0.068241
Lg. Intestine	0.114878	0.081181	0.065488	0.069404
Muscle	0.076811	0.096078	0.054596	0.049649
Fat	0.907396	0.032577	0.035763	0.036914
Calvaria	0.181434	0.237983	0.322224	0.186745
Brain	0.027033	0.032088	0.043893	0.065779

t = 4 h	n1	n2	n3	n4
Blood	0.042119	0.041018	0.038674	0.053364
Heart	0.042844	0.053032	0.036666	0.045187
Lungs	0.041294	0.040158	0.042127	0.044061
Liver	0.078102	0.063846	0.054529	0.069627
Spleen	0.079473	0.059053	0.05195	0.081098
Kidney	1.038842	0.781203	0.656854	0.963115
Stomach	0.601321	0.146043	0.299731	0.692344
Lg. Intestine	9.728082	1.341974	7.293979	10.60601
Muscle	0.056514	0.045633	0.041528	0.033938
Fat	0.025782	0.020914	0.017206	0.033765
Calvaria	0.12483	1.358133	0.225513	0.240393
Brain	0.019922	0.067867	0.042717	0.019529

Table S6. Organ distribution of ^{225}Ac–PYTA after intravenous injection in mice (%ID/g).

t = 15 min	n1	n2	n3	n4
Blood	1.173272	1.21113	0.67148	1.500477
Heart	0.351432	0.431206	0.397345	1.286487
Lungs	0.521298	0.673906	0.929379	1.262782
Liver	0.77467	0.893213	0.739594	1.014385
Spleen	0.165084	0	0.417035	0.267267
Kidneys	2.040084	2.532671	2.129184	5.143537
Stomach	0.082587	0.236874	0.239382	1.84617
Lg. Intestine	0.114593	0.278554	0.370487	0.316469
Muscle	0.194934	0.201244	0.374455	0.370234
Fat	0.148751	0.063538	0.201985	0.129948
Skin	0.515429	0.472025	1.133798	0.952285
Calvaria	0.298396	0.205208	0.065161	0.317577
Brain	0.057892	0.017167	0.037416	0.234219

t = 1 h	n1	n2	n3	n4
Blood	0.198172	0.119656	0.020577	0.093215
Heart	0.069758	0	0	0.056769
Lungs	0.137186	0.134725	0.061418	0.054206
Liver	0.086206	0.132574	0.081484	0.104757
Spleen	0.073788	0.079669	0.125855	0.129377
Kidneys	0.432342	1.184163	0.466559	0.560756
Stomach	0.28989	0.019814	0.038091	0.066131
Lg. Intestine	0	0.034036	0.017037	0.033469
Muscle	0.09061	0.02203	0.012177	0
Fat	0.078649	0	0.025922	0.051226
Skin	0.18902	0.3604	0.03456	0.08164
Calvaria	0.129643	0.043402	0	1.290521
Brain	0.002493	0.011323	0.166678	0

t = 24 h	n1	n2	n3	n4
Blood	0	0.047524	0	0
Heart	0	0.008842	0.043272	0
Lungs	0	0	0.00668	0.020314
Liver	0	0.003748	0.030623	0
Spleen	0.157768	0.082952	0.070438	0.002567
Kidneys	0.238479	0.158461	0.15545	0.20715
Stomach	0.0000739	0.00806	0	0.024398
Lg. Intestine	0.033317	0.077594	0.11109	0.099018
Muscle	0	0.040048	0.071953	0
Fat	0	0.105309	0.180378	0.386826
Skin	0	0	0	0
Calvaria	0	0.047676	0.127564	0
Brain	0	0	0.02562	0

t = 48 h	n1	n2	n3	n4
Blood	0	0	0	0.022155
Heart	0	0	0	0
Lungs	0	0	0	0
Liver	0.010188	0.019444	0	0
Spleen	0	0.033296	0.033367	0
Kidneys	0.082178	0.081183	0.103577	0.003819
Stomach	0	0	0	0
Lg. Intestine	0.060154	0.071331	0.017096	0.0127
Muscle	0.027144	0	0	0.045711
Fat	0	0.178409	0.047879	0.073222
Skin	0.094187	0	0	0.304298
Calvaria	0	0	0	0
Brain	0	0	0	0

9. References

1 X. Zeng, D. Coquiére, A. Alenda, E. Garrier, T. Prangé, Y. Li, O. Reinaud and I. Jabin, *Chem. Eur. J.*, 2006, **12**, 6393–6402.
2 M. Mato-Iglesias, A. Roca-Sabio, Z. Pálinkás, D. Esteban-Gómez, C. Platas-Iglesias, É. Tóth, A. de Blas and T. Rodríguez-Blas, *Inorg. Chem.*, 2008, **47**, 7840–7851.
3 A. Roca-Sabio, M. Mato-Iglesias, D. Esteban-Gómez, É. Toth, A. de Blas, C. Platas-Iglesias and T. Rodríguez-Blas, *J. Am. Chem. Soc.*, 2009, **131**, 3331–3341.
4 L. Valencia, J. Martinez, A. Macías, R. Bastida, R. A. Carvalho and C. F. G. C. Geraldes, *Inorg. Chem.*, 2002, **41**, 5300–5312.
5 G. L. Rothermel Jr., L. Miao, A. L. Hill and S. C. Jackels, *Inorg. Chem.*, 1992, **31**, 4854–4859.
6 G. Kresse, *J. Non-Cryst. Solids*, 1995, **192–193**, 222–229.
7 G. Kresse and J. Furthmüller, *Comput. Mater. Sci.*, 1996, **6**, 15–50.
8 P. E. Blöchl, *Phys. Rev. B*, 1994, **50**, 17953–17979.
9 G. Kresse and D. Joubert, *Phys. Rev. B*, 1999, **59**, 1758–1775.
10 J. P. Perdew, K. Burke and M. Ernzerhof, *Phys. Rev. Lett.*, 1996, **77**, 3865–3868.
11 S. Grimme, J. Antony, S. Ehrlich and H. Krieg, *J. Chem. Phys.*, 2010, **132**, 154104.
12 C. F. Macrae, P. R. Edgington, P. McCabe, E. Pidcock, G. P. Shields, R. Taylor, M. Towler and J. van de Streek, *J. Appl. Crystallogr.*, 2006, **39**, 453–457.
13 P. Pulay, *Chem. Phys. Lett.*, 1980, **73**, 393–398.
14 H. Sun, S. J. Mumby, J. R. Maple and A. T. Hagler, *J. Am. Chem. Soc.*, 1994, **116**, 2978–2987.
15 W. G. Hoover, *Phys. Rev. A*, 1985, **31**, 1695–1697.
16 S. Nosé, *J. Chem. Phys.*, 1984, **81**, 511–519.
17 G. M. Sheldrick, *Acta Crystallogr. Sect. C Struct. Chem.*, 2015, **71**, 3–8.
18 O. V. Dolomanov, L. J. Bourhis, R. J. Gildea, J. A. K. Howard and H. Puschmann, *J. Appl. Crystallogr.*, 2009, **42**, 339–341.
19 N. Benabdallah, H. Zhang, R. Unnerstall, A. Fears, L. Summer, M. Fassbender, B. E. Rodgers, D. Abou, V. Radchenko and D. L. J. Thorek, *EJNMMI Res.*, 2023, **13**, 17.
20 A. Hu, M. E. Simms, V. Kertesz, J. J. Wilson and N. A. Thiele, *Inorg. Chem.*, 2022, **61**, 12847–12855.

10. Appendices

A. Chelator characterization data

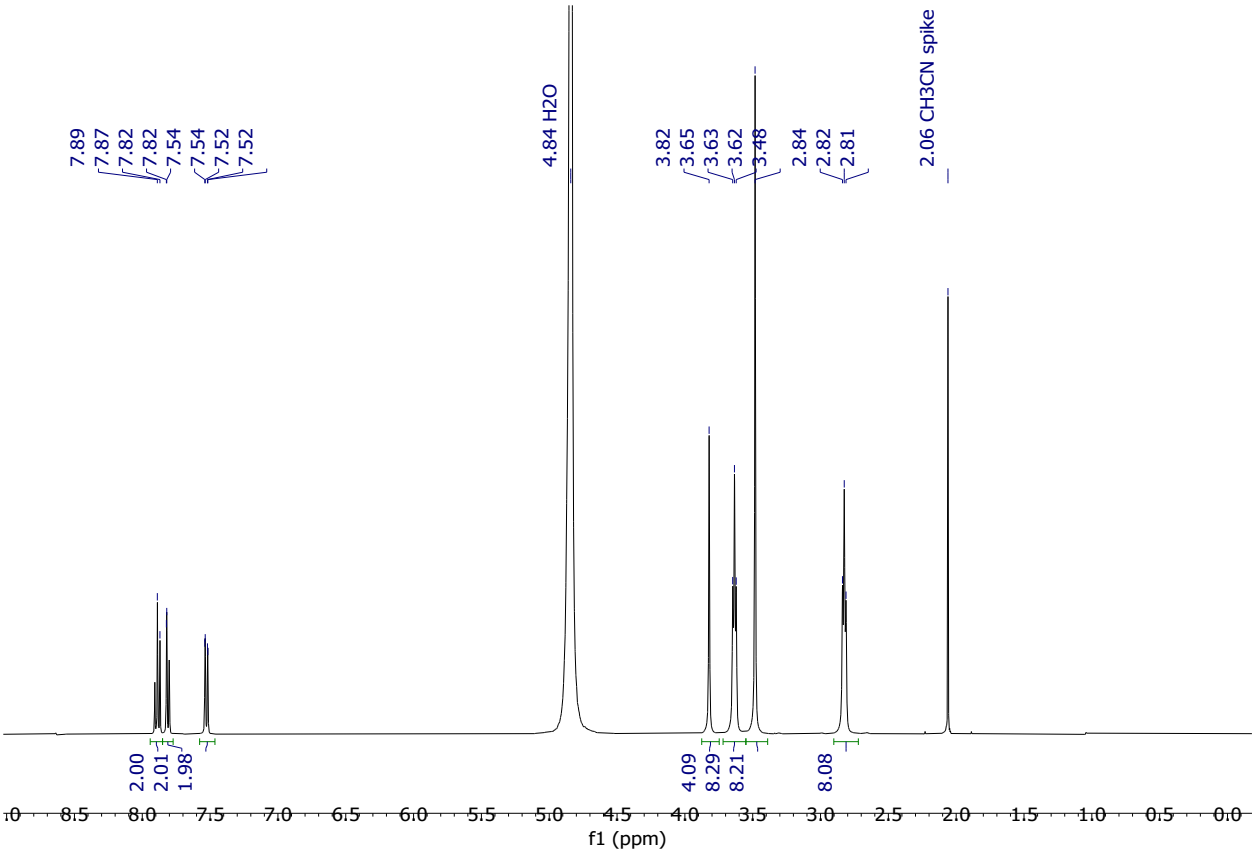

Figure A1. ^{1}H NMR spectrum of macropa. 400 MHz, D_2O + aq. NaOH, app pD >8.

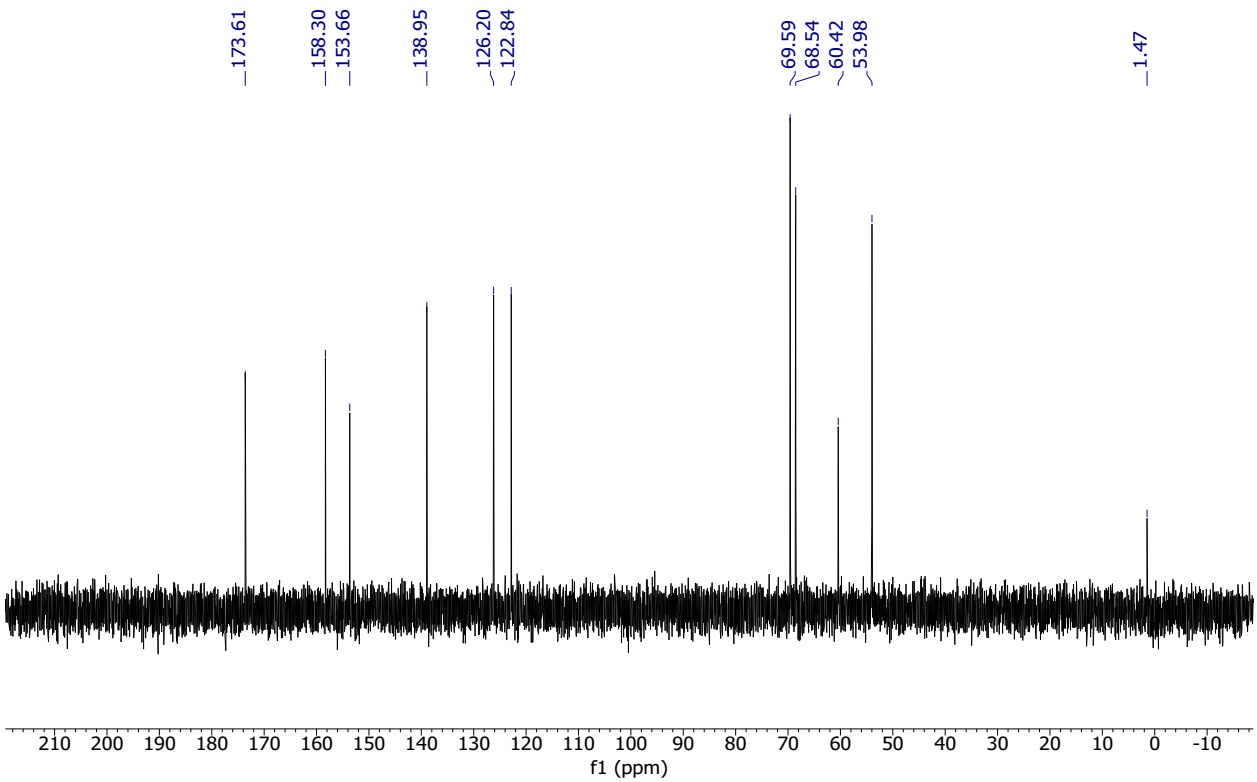

Figure A2. $^{13}C\{^{1}H\}$ NMR spectrum of macropa. 101 MHz, D_2O + aq. NaOH, app pD >8.

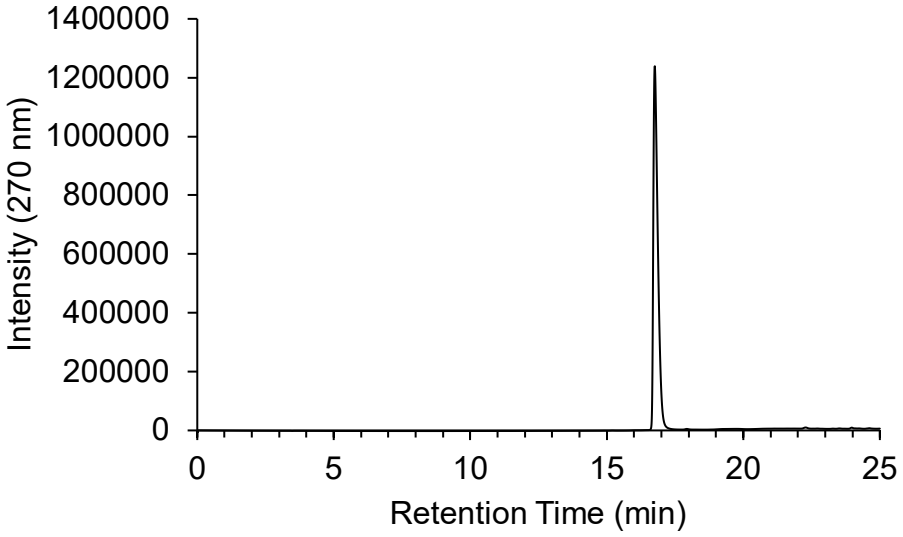

Figure A3. HPLC chromatogram of macropa. Retention time (t_R) = 16.76 min using a binary MeOH/H_2O mobile phase containing 0.1% TFA (program: 10% MeOH for 5 min, followed by a linear gradient to 100% MeOH over 20 min).

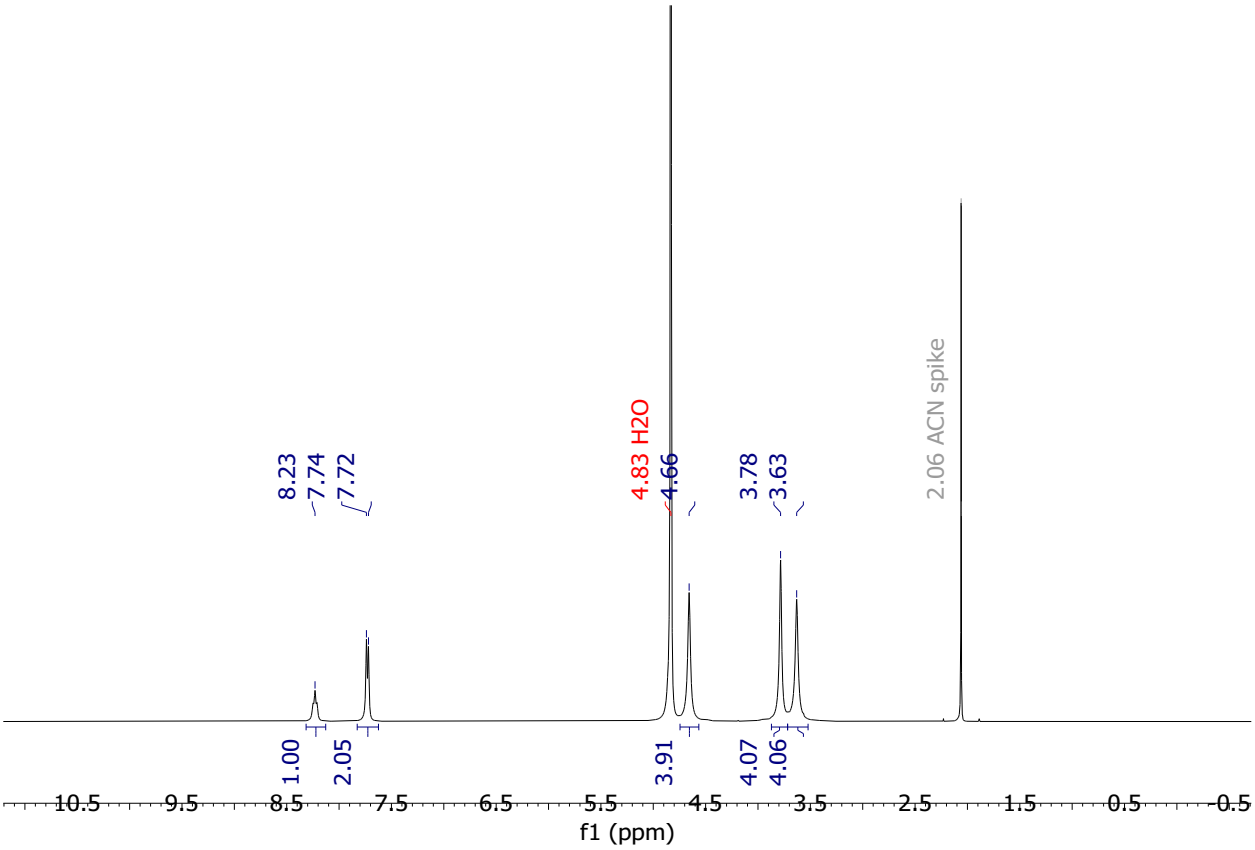

Figure A4. ^{1}H NMR spectrum of PYTA. 400 MHz, D_2O, app pD 1–2 by litmus paper.

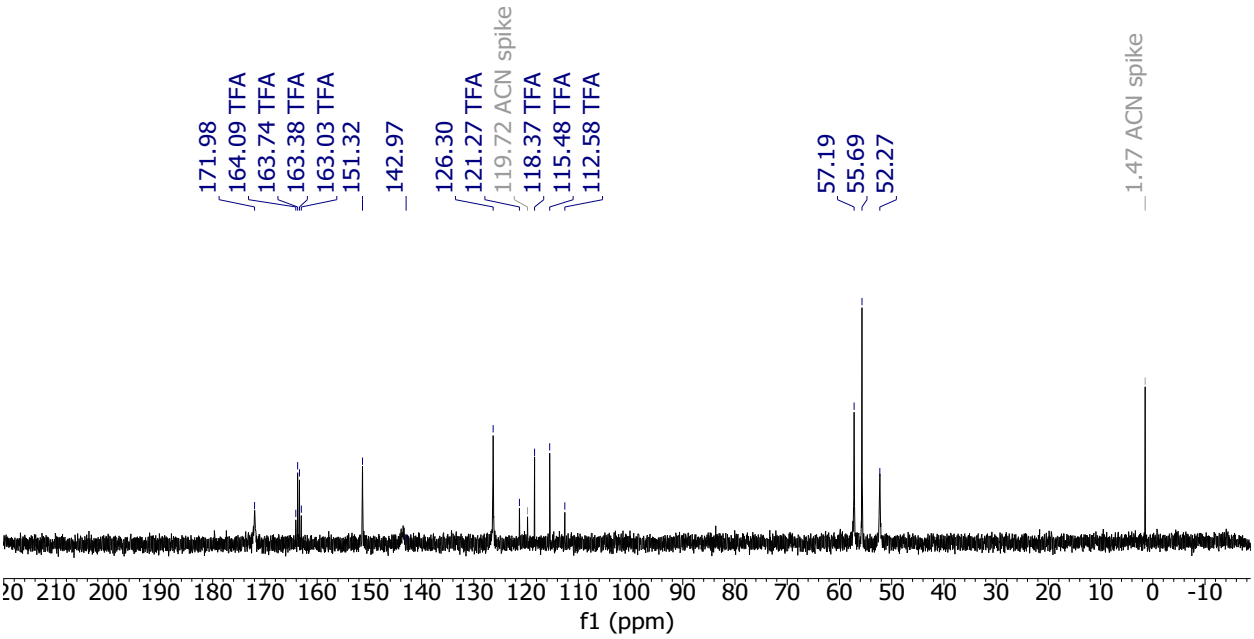

Figure A5. $^{13}C\{^{1}H\}$ NMR spectrum of PYTA. 101 MHz, D_2O, app pD 1–2 by litmus paper.

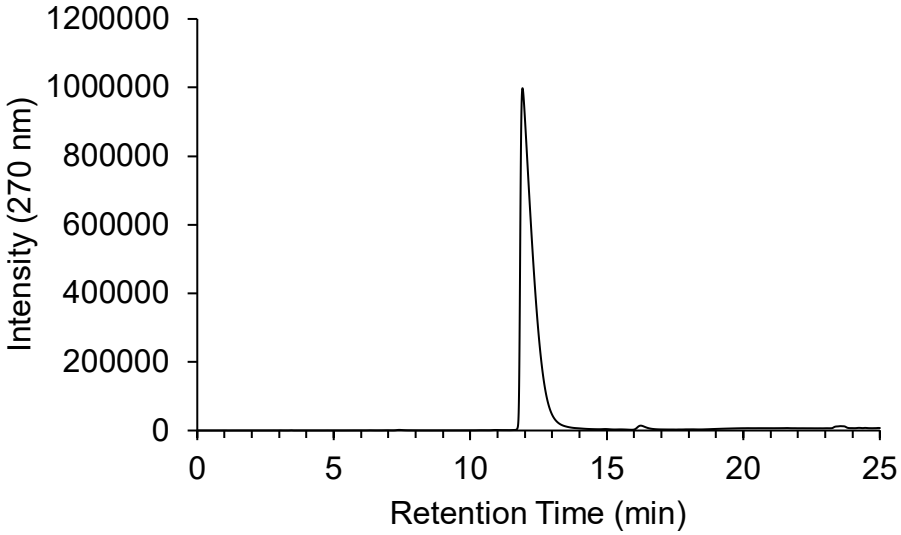

Figure A6. HPLC chromatogram of PYTA. Retention time (t_R) = 11.91 min using a binary MeOH/H_2O mobile phase containing 0.1% TFA (program: 10% MeOH for 5 min, followed by a linear gradient to 100% MeOH over 20 min).

B. HPGe gamma-ray spectra

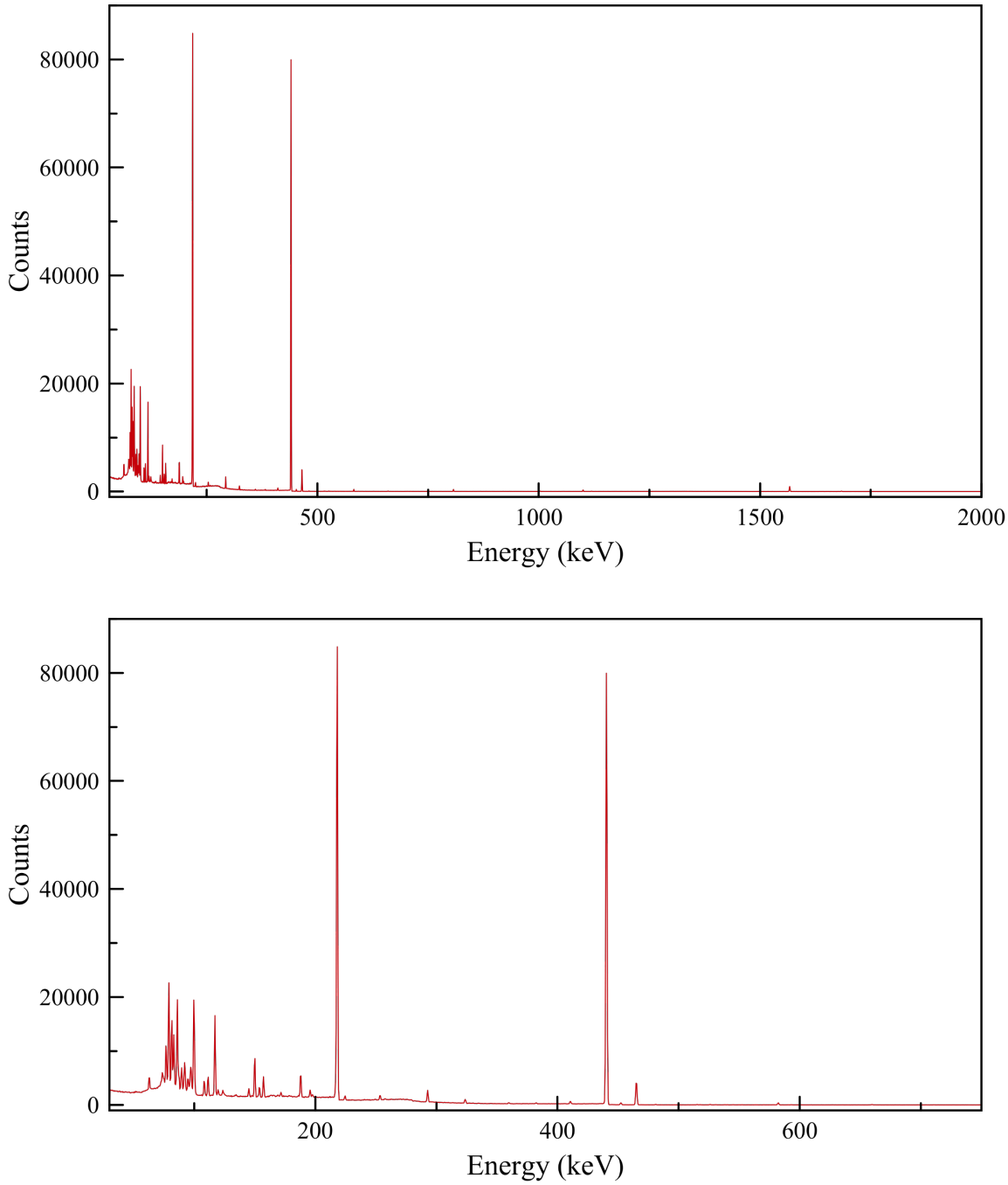

Figure B1. HPGe gamma-ray spectra of ^{225}Ac used in this work. Top: full view. Bottom: focused view.

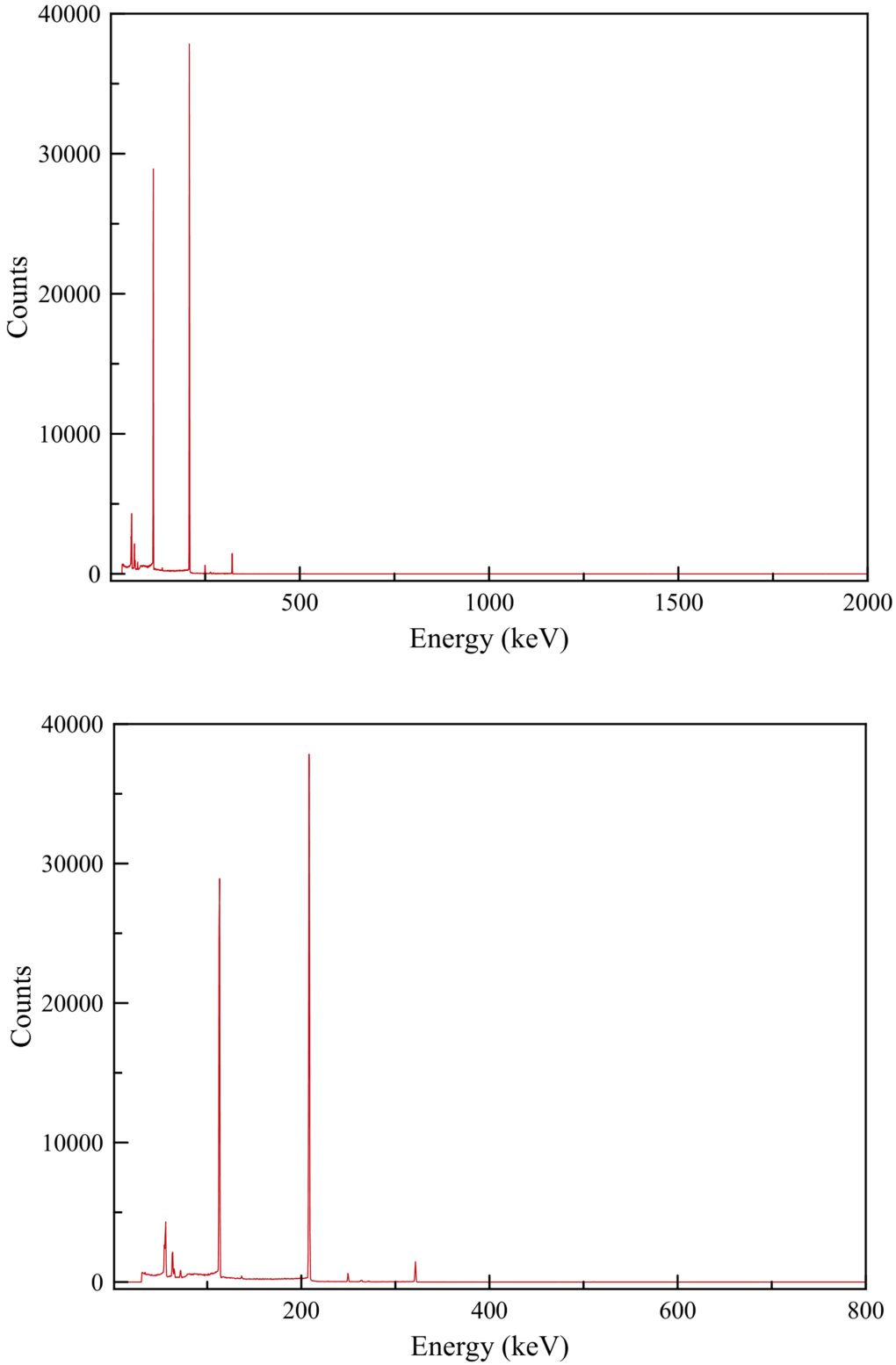

Figure B2. HPGe gamma-ray spectra of ^{177}Lu used in this work. Top: full view. Bottom: focused view.

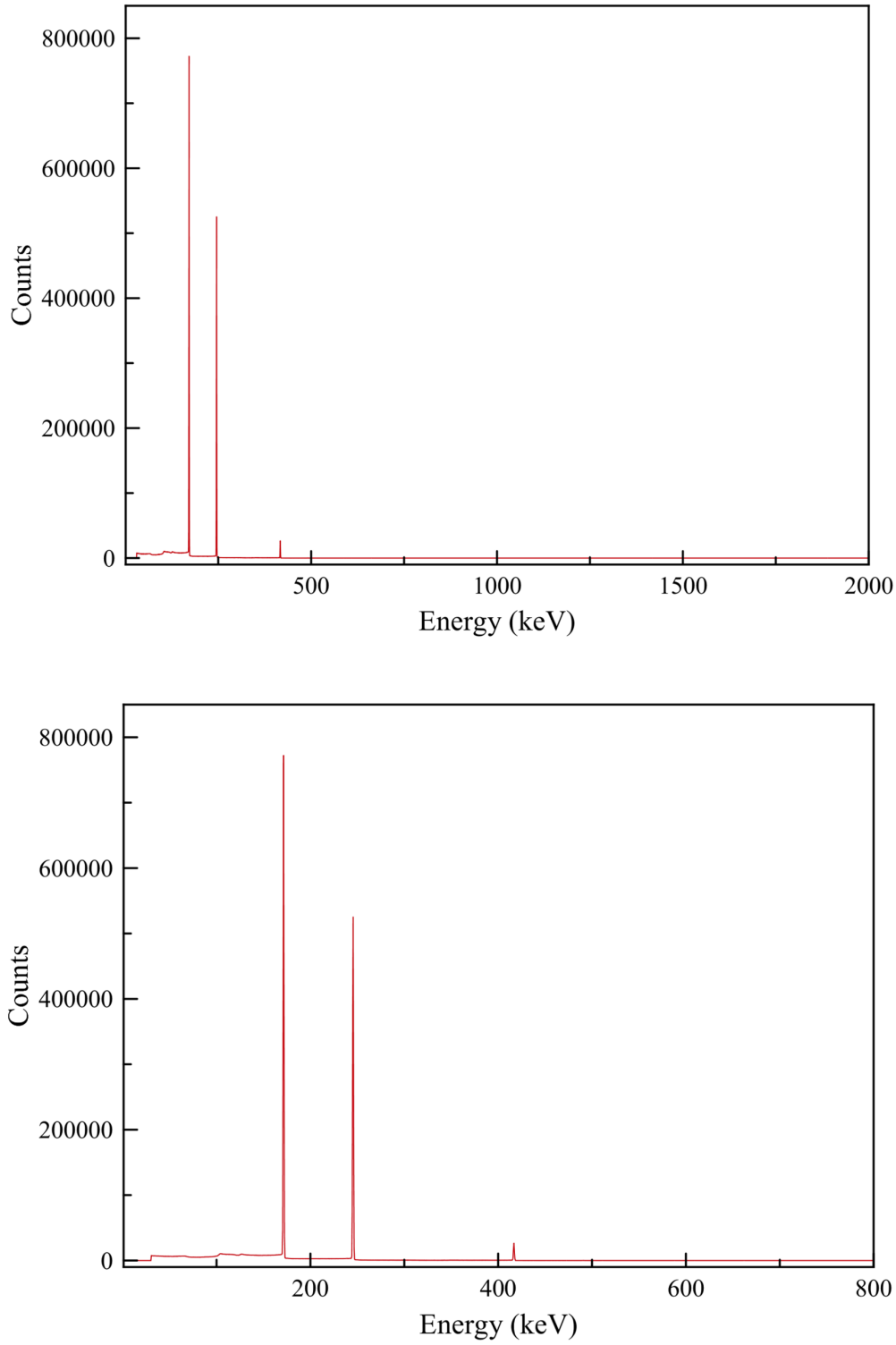

Figure B3. HPGe gamma-ray spectra of ^{111}In used in this work. Top: full view. Bottom: focused view.

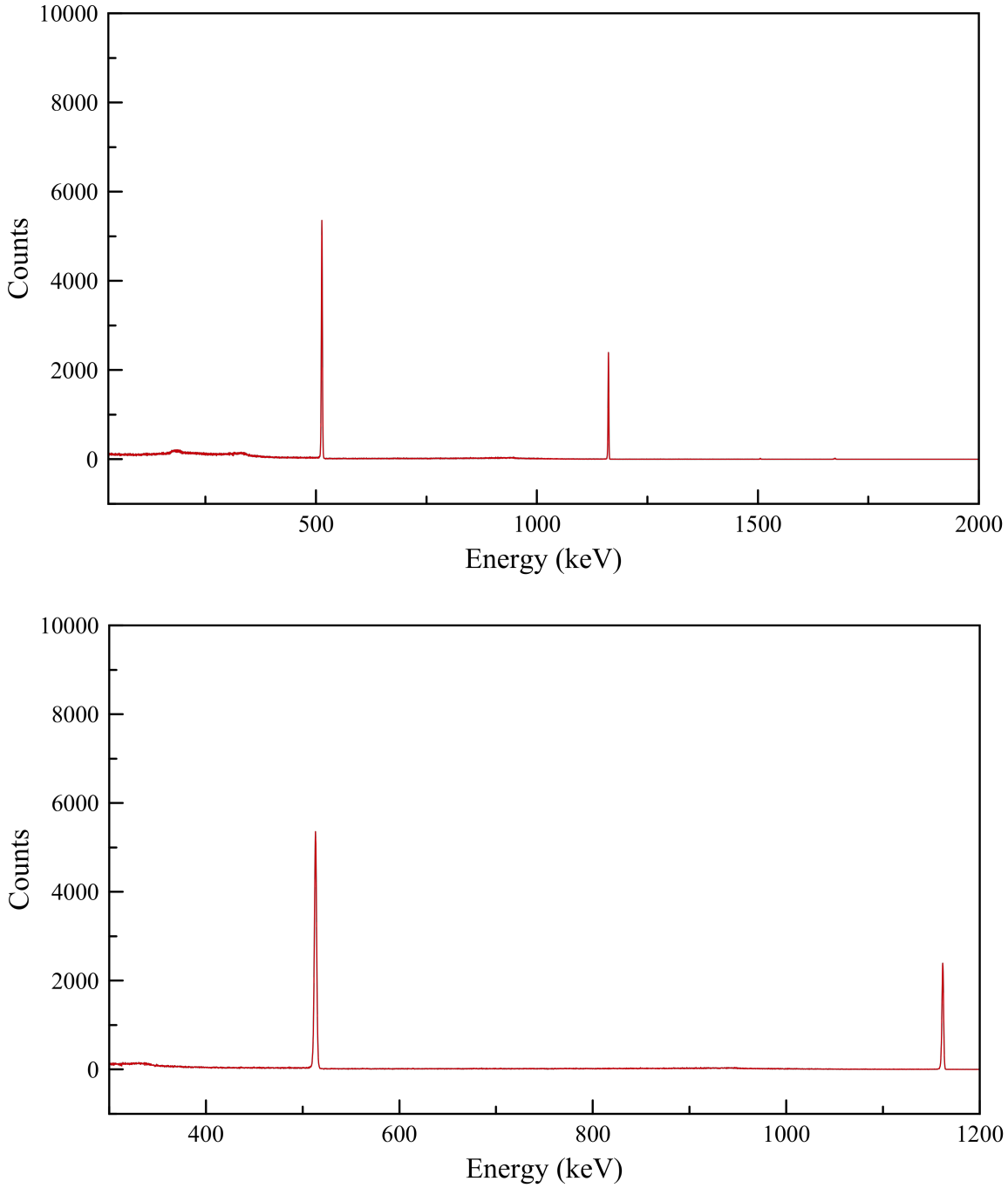

Figure B4. HPGe gamma-ray spectra of ^{44}Sc used in this work. Top: full view. Bottom: focused view.